Revisiting the spectral analysis for high-order spectral discontinuous methods

Julien Vanharen [a,*], Guillaume Puigt [a], Xavier Vasseur [b],
Jean-François Boussuge [a], Pierre Sagaut [c]

[a] *Centre Européen de Recherche et de Formation Avancée en Calcul Scientifique (CERFACS), 42 avenue Gaspard Coriolis, 31057 Toulouse Cedex 01, France*
[b] *ISAE-SUPAERO, 10 avenue Edouard Belin, BP 54032, 31055 Toulouse Cedex 4, France*
[c] *Aix Marseille Univ, CNRS, Centrale Marseille, M2P2 UMR 7340, 13451 Marseille, France*

ABSTRACT

The spectral analysis is a basic tool to characterise the behaviour of any convection scheme. By nature, the solution projected onto the Fourier basis enables to estimate the dissipation and the dispersion associated with the spatial discretisation of the hyperbolic linear problem. In this paper, we wish to revisit such analysis, focusing attention on two key points. The first point concerns the effects of time integration on the spectral analysis. It is shown with standard high-order Finite Difference schemes dedicated to aeroacoustics that the time integration has an effect on the required number of points per wavelength. The situation depends on the choice of the coupled schemes (one for time integration, one for space derivative and one for the filter) and here, the compact scheme with its eighth-order filter seems to have a better spectral accuracy than the considered dispersion-relation preserving scheme with its associated filter, especially in terms of dissipation. Secondly, such a coupled space–time approach is applied to the new class of high-order spectral discontinuous approaches, focusing especially on the Spectral Difference method. A new way to address the specific spectral behaviour of the scheme is introduced first for wavenumbers in $[0, \pi]$, following the Matrix Power method. For wavenumbers above π, an aliasing phenomenon always occurs but it is possible to understand and to control the aliasing of the signal. It is shown that aliasing depends on the polynomial degree and on the number of time steps. A new way to define dissipation and dispersion is introduced and applied to wavenumbers larger than π. Since the new criteria recover the previous results for wavenumbers below π, the new proposed approach is an extension of all the previous ones dealing with dissipation and dispersion errors. At last, since the standard Finite Difference schemes can serve as reference solution for their capability in aeroacoustics, it is shown that the Spectral Difference method is as accurate as (or even more accurate) than the considered Finite Difference schemes.

* Corresponding author.
 E-mail addresses: julien.vanharen@cerfacs.fr (J. Vanharen), guillaume.puigt@cerfacs.fr (G. Puigt), xavier.vasseur@isae.fr (X. Vasseur),
jean-francois.boussuge@cerfacs.fr (J.-F. Boussuge), pierre.sagaut@univ-amu.fr (P. Sagaut).

1. Introduction

Because of the continuous growth of available computational resources during the last decade, there was an increased interest in performing Large Eddy Simulation – LES – to solve industrial problems. Among these problems, aeroacoustics requires to compute and to transport accurately pressure waves around complex geometries and over a long distance. Many classes of schemes were proposed to perform LES during the last 30 years, depending on the underlying mathematical framework considered to discretise the Navier–Stokes equations.

First, in the context of Finite Difference – FD – formalism, high-order centred schemes for structured grids were built following the Taylor's expansion technique and their accuracy was compared with the one of spectral methods [1]. Any (high) order of accuracy can be attained but the number of degrees of freedom to update the solution at one point can be large. Two optimisations of FD schemes were introduced: the compact formulation of Lele [2] that leads to a spectral-like resolution and the Dispersion–Relation–Preserving – DRP – technique of Tam and Webb [3] dedicated to aeroacoustics. The compact approach links several derivatives with unknowns located closely. By this way, a linear (implicit) system of equations links all derivatives with unknowns. For a given accuracy, the stencil of DRP schemes is larger than for the standard FD approach and the extra unknowns enable to control the numerical properties of the scheme: dissipation and dispersion. Both approaches being centred, they are non dissipative and a filter stabilizes the computations by dissipating wavenumbers. In this paper, we consider compact and DRP schemes as standard ingredients for LES and it is assumed that they will provide reference results.

More recently, a new generation of high-order techniques denoted as *spectral discontinuous* emerged. Following the pioneering work of Reed and Hill [4], the Discontinuous Galerkin – DG – formulation was first applied to hyperbolic equations by Cockburn, Shu and co-authors [5–7] and opened many years of research and papers (see [8] as an example of reference book on DG method). The idea is to solve problems defined in the weak form inside any mesh cell, without requiring the solution to be continuous at the mesh interfaces. At the interface, the fluxes are computed using standard Riemann solvers, as in Finite Volume – FV – formalism. Therefore, the FV flux computation enables the coupling of the weak problems in surrounding cells and the FV fluxes make information going across mesh interfaces. Several alternative high-order methods have been recently introduced. Following the staggered-grid multidomain spectral method [9] for structured grids, Liu, Vinokur and Wang [10,11] introduced the Spectral Difference – SD – method aiming at a simpler to implement and more efficient method than the current state of the art for the DG method. The approach was then extended to mixed elements [12]. The SD method takes benefit of the resolution of the strong differential form of the equations, as in FD, but does not assume that the solution is continuous on the whole mesh, as in FV. Another way to define a high-order polynomial reconstruction follows the definition of averaged quantities, as in FV. With the Spectral Volume – SV – approach [13–17], a polynomial reconstruction is defined inside any cell using the averaged quantities over sub-cells built by subdivision of the initial mesh elements. As before, several Riemann problems are solved on mesh boundaries since the solution polynomials are not required to be continuous at mesh interfaces. Finally, the Flux Reconstruction method introduced in 2007 by Huynh [18] solves the strong form of the equation. It can be seen as a collocated Spectral Difference scheme but the main difference occurs in the definition of the flux polynomial: now, a lifting operator [19–22] is introduced to increase the polynomial degree of the initial flux polynomial by one. This is mandatory to recover the required polynomial degree after the computation of the divergence (hyperbolic) term. The main advantage of FR method is its ability to recover SD, SV and DG approaches for the linear advection equation, depending on the lifting operator [23]. Compared to the standard schemes for structured grids, the major advantage of DG, SV, SD and FR methods lies in their natural ability to handle unstructured meshes, which is a prerequisite to treat complex geometries. Moreover, such schemes use a very compact stencil, defined locally inside any mesh cell. This is also an advantage in terms of high performance computing required by massively-parallel LES.

When dealing with aeroacoustics, the first question to answer concerns the spectral accuracy of the chosen scheme: the key point concerns the required number of grid points per wavelength. The spectral analysis [24] consists of dealing with the space derivative and in comparing the numerical spatial derivative with the theoretical derivative, after projection onto the Fourier basis. This analysis is performed on the linear advection equation in a periodic domain with a harmonic initial solution:

$$\begin{cases} \dfrac{\partial u}{\partial t} + c \dfrac{\partial u}{\partial x} = \dfrac{\partial u}{\partial t} + c\, \mathbb{D}(u) = 0 \\ u_0(x) = u(0, x) = \exp(jkx) \text{ with } j^2 = -1, \end{cases} \tag{1}$$

where the function $u(x, t)$ is the unknown, c the constant advective velocity, k the constant wavenumber and $\mathbb{D}$ represents the spatial derivative operator. As a consequence, Eq. (1) will play an important role and for sake of clarity, the notation for the unknowns will be kept unchanged along the whole document.

The formulation of the Fourier spectral analysis makes the analysis simple for standard schemes based on Finite Difference paradigm. This is due to the fact that the degrees of freedom are coupled by the numerics and not by the method itself. As introduced by Hu et al. in 1999 [25] for the DG method, the situation is more complex for spectral discontinuous methods. For DG method, the authors show that the degrees of freedom are coupled by the definition of the local polynomial – inside any mesh cell. Finally, the Fourier analysis can be performed as for FD approach but the final equation changes. Instead of one equation giving the complex-valued numerical wavenumber, one obtains, even for a scalar equation,

a set of linear equations. Depending on the polynomial degree p, $p + 1$ waves are solutions of the linear set of equations. In [25], it is then explained that among the $p + 1$ waves travelling at different phase speeds, one mode is the *physical mode* as its frequency approximates the exact dispersion relation for a range of wavenumbers, while the others are the *parasite modes* due to the scheme. In other words, the solution is the superposition of one physical mode and p parasite modes. Such results were also obtained by Zhang et al. for three different formulations of the DG method [26]. The same kind of analysis with $p + 1$ waves, one physical mode and p parasite modes, was also proposed for the SV approach [27], for the SD approach [28] and for the FR technique [20,29,30]. Finally, even if the occurrence of parasite modes is demonstrated, the proposed analysis does not explain the role of these parasite modes. Moreover, even if it can be proved that the eigenvalues of the system are periodic (with a period of 2π), the spectral analysis presented in [20,25–30] shows that the spectral behaviour, playing with the wavenumber and the order p of the polynomials, is no longer 2π-periodic. This point is clearly not in agreement with mathematical requirements.

In this paper, we introduce a new way to perform the Fourier spectral analysis for polynomial discontinuous methods and we compare the accuracy of the SD technique with two standard centred and stabilized FD schemes, the compact scheme of Lele [2] and a DRP scheme developed by Bogey and Bailly [31]. The remainder of this paper unfolds as follows. In Sec. 2, the space–time Fourier spectral analysis is applied to the considered spatial FD schemes coupled with a low-storage second-order Runge Kutta scheme. In Sec. 3, a new analysis of the spectral Fourier approach for spectral discontinuous methods is introduced and applied to the SD method. In Sec. 4, we explicitly address the case of a wavenumber larger than π and we give the analysis in terms of number of points per wavelength for the SD method. Before concluding, standard FD schemes and SD scheme are finally compared in Sec. 5.

2. Space–time spectral analysis for high-order Finite Difference methods

As an introduction, we briefly explain how the space–time spectral analysis is performed. This advanced method is then applied to two Finite Difference schemes. The results obtained in this section will notably play an important role later for purpose of comparison with the new results shown in Sec. 3.

2.1. Space and time discretisations

Let us introduce a one-dimensional domain decomposed of elements with uniform length Δx. In 1D, any convection equation with a constant advection velocity is linear and the key point concerns the definition of the numerical derivative. Let u_i be the discrete unknown at the point i and u_i' its derivative at the same location. The length of the computational domain is not taken into consideration: the goal is to derive scheme expressions for a given point far from the boundary (in order to have access to the whole scheme stencil). For numerical simulations, the system of equations will be closed by applying periodic boundary conditions but this assumption is not mandatory to derive analytical expressions far from the boundary. In the following, two schemes frequently applied to aeroacoustics simulations are considered.

The first scheme is the sixth-order compact scheme of Lele [2] denoted CS6. This scheme is purely centred and for stabilization, damping high frequency waves is mandatory. Here, the compact filter denoted CF8 is the eighth-order filter designed by Visbal and Gaitonde [32]. The Lele's sixth-order compact scheme CS6 approximates the first-order spatial derivative with:

$$\frac{1}{3}u_{i-1}' + u_i' + \frac{1}{3}u_{i+1}' = \frac{14}{9}\frac{u_{i+1} - u_{i-1}}{2\Delta x} + \frac{1}{9}\frac{u_{i+2} - u_{i-2}}{4\Delta x}, \tag{2}$$

while the eighth-order compact filter CF8 designed by Visbal and Gaitonde is defined by:

$$\alpha_f u_{i-1}^f + u_i^f + \alpha_f u_{i+1}^f = \sum_{l=0}^{4} b_l \frac{u_{i+l} + u_{i-l}}{2}, \tag{3}$$

where the superscript f means filtered. The b_l coefficients in Eq. (3) are given in Table 14. The filter coefficient α_f is equal to 0.47. This numerical setup is used by, *e.g.*, Aikens et al. [33] or Le Bras et al. [34].

The second scheme of interest is the optimised fourth-order DRP scheme designed by Bogey and Bailly [31], denoted FDo11p. It uses a symmetric stencil with 11 points and its expression is:

$$u_i' = \frac{1}{\Delta x} \sum_{l=-5}^{5} a_l u_{i+l}. \tag{4}$$

The scheme is stabilized by an optimised sixth-order filter denoted SFo11p [35] which is defined on the same stencil:

$$u_i^f = u_i - \sigma_d \sum_{l=-5}^{5} d_l u_{i+l}. \tag{5}$$

Table 1
CFL stability for the RKo6s–SFo11p–FDo11p and RKo6s–CF8–CS6 combinations.

Runge–Kutta	Filter	Scheme	ν
RKo6s	SFo11p	FDo11p	2.053740
RKo6s	CF8	CS6	1.997980

The optimised coefficients for the FDo11p scheme (a_l) and for the SFo11p filter (d_l) are given in Table 15. σ_d in Eq. (5) is generally chosen such that $\sigma_d = 1.0$ [35].

The advection equation (1) is now time-marched using a standard explicit time integration procedure based on the Runge–Kutta Method. In the whole paper, the low-storage DRP second-order six-stage Runge–Kutta (RKo6s) scheme of Bogey and Bailly [31] is chosen. For completeness, the Runge–Kutta coefficients are given in Table 16.

The full space and time integration is as follows. First, the spatial derivative u_i' is computed thanks to the numerical scheme (either FDo11p or CS6). Then, the standard Runge–Kutta time integration is performed and finally, the filter (either SFo11p or CF8) is applied to the updated solution.

2.2. Space–time analysis

The analysis being performed in both space and time, $u(x, t)$ is discretised by $u_i^n = u(i\Delta x, n\Delta t)$, where the index i (resp. n) refers to space (resp. time) position and Δt to the time step. The fully discrete space–time scheme then reads:

$$u_i^{n+1} = u_i^n + \sum_{l=1}^{6} \gamma_l \left(-c\Delta t \mathbb{D}(u_i^n) \right)^l, \tag{6}$$

where $\mathbb{D}$ is the derivative operator introduced in Eq. (1).

Introducing the Courant–Friedrichs–Lewy – CFL – number defined by $\nu = c\Delta t/\Delta x$ and the discretised normal mode

$$u_i^n = \exp\left(-jn\omega\Delta t + ji k\Delta x \right)$$

into Eq. (6) and applying the filter transfer function, the expression of the dispersion relation of the space–time scheme with filtering is:

$$\exp\left(-j\omega\Delta t \right) = \mathcal{F}(k\Delta x) \left(1 + \sum_{l=1}^{6} \gamma_l \left(-j\nu k_m\Delta x \right)^l \right). \tag{7}$$

Eq. (7) contains two new quantities. k_m represents the modification of the spatial mode k when the spatial scheme is applied. Moreover, $\mathcal{F}(k\Delta x)$ represents the transfer function associated to either CF8 or SFo11p filters. The analytical expressions for $\mathcal{F}$ and the analytical relations between k_m and k are given in Appendix A for consistency.

Such a dispersion relation must be compared with the exact one $\omega = kc$. The corresponding dimensionless dispersion relation is $\omega\Delta t = \nu k\Delta x$. Let us now introduce:

$$\mathcal{G}(k\Delta x) = \mathcal{F}(k\Delta x) \left(1 + \sum_{l=1}^{6} \gamma_l \left(-j\nu k_m\Delta x \right)^l \right), \tag{8}$$

$$\varphi = -\arg\left(\mathcal{G} \right) / \nu \in]-\pi, \pi], \tag{9}$$

$$\rho = |\mathcal{G}|. \tag{10}$$

For a non dispersive scheme, φ is equal to $\omega\Delta t/\nu = k\Delta x$. For a non dissipative scheme, ρ is equal to 1. $\rho > 1$ gives amplification, whereas $\rho < 1$ gives dissipation. Such a coupled space–time approach has been previously introduced in [36–38].

Remark. The quantities ρ and φ are defined for one iteration of the time integration process.

2.3. Stability analysis based on CFL criterion

The space–time discretisation is stable under a CFL condition. Before performing the Fourier analysis, the maximum CFL number for stable computation is computed. Starting from Eq. (6), the iterative process to find u_i^n is convergent if ρ is strictly lower than 1. Looking for the largest time step to maintain ρ strictly lower than 1 for all $k\Delta x$ is an optimisation problem and the stability limits (that we obtained) are summarized in Table 1.
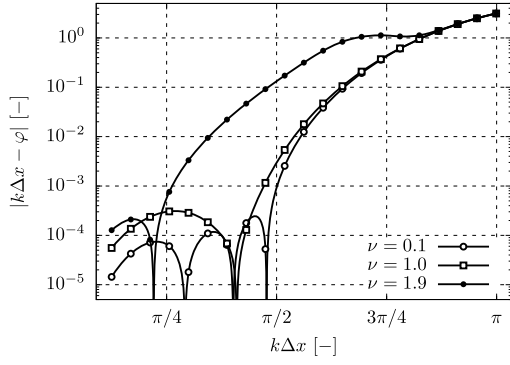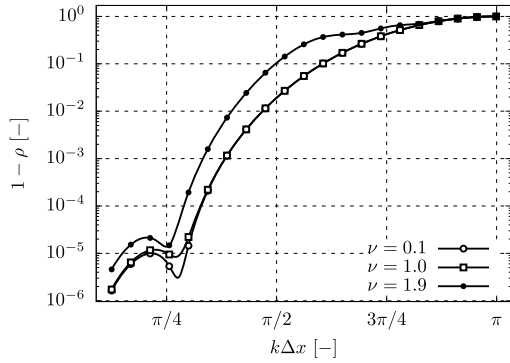
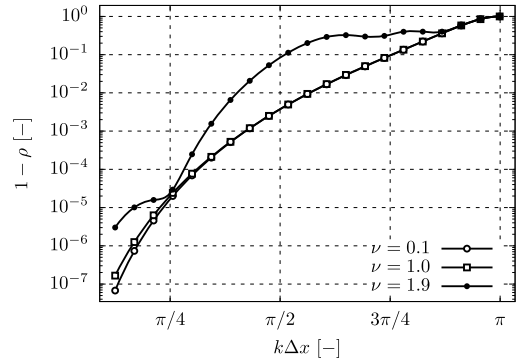(a) *Dispersion error using RKo6s-SFo11p-FDo11p combination.*
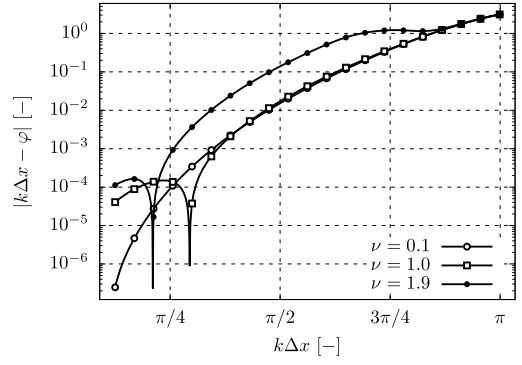
(b) *Dispersion error using RKo6s-CS6 combination.*

Fig. 1. Effect of time integration on dispersion for the proposed FD schemes.

(a) *Dissipation error using RKo6s-SFo11p-FDo11p combination.*

(b) *Dissipation error using RKo6s-CS6 combination.*

Fig. 2. Effect of time integration on dissipation for the proposed FD schemes.

2.4. Spectral analysis

Three CFL numbers (0.1, 1.0 and 1.9, respectively) are chosen in agreement with the stability constraints in Table 1 and both dispersion and dissipation are estimated from Eq. (8). Numerical results are shown in Fig. 1 and Fig. 2 for dispersion and dissipation, respectively. These curves show that the spectral behaviour changes with the CFL number and as highlighted in the next section, this change in spectral behaviour has a strong impact on the number of grid points per wavelength.

2.5. Number of points per wavelength (PPW)

The number of points per wavelength is representative of the resolution power of any numerical scheme. The criteria proposed by Bogey and Bailly [31] are chosen to measure the maximum wavenumber properly (resp. accurately), defined with subscript p (resp. with subscript a) and calculated for both dispersion and dissipation (superscript ϕ and E respectively). The four criteria are expressed as an optimisation problem. For the dispersion, the optimisation problems are:

Look for $k_p^\phi \Delta x$ solution of: $\max\limits_{k\Delta x}|k\Delta x - \varphi| \leqslant 5\pi \times 10^{-4}$,

Look for $k_a^\phi \Delta x$ solution of: $\max\limits_{k\Delta x}|k\Delta x - \varphi| \leqslant 5\pi \times 10^{-5}$.

Similarly, the optimisation problems for dissipation are:

Look for $k_p^E \Delta x$ solution of: $\max\limits_{k\Delta x}|1 - \rho| \leqslant 2.5 \times 10^{-3}$,

Look for $k_a^E \Delta x$ solution of: $\max\limits_{k\Delta x}|1 - \rho| \leqslant 2.5 \times 10^{-4}$.

Table 2
Number of points per wavelength for the space–time coupled approach using the RKo6s–SFo11p–FDo11p combination.

ν	$\lambda_p^\phi/\Delta x$	$\lambda_a^\phi/\Delta x$	$\lambda_p^E/\Delta x$	$\lambda_a^E/\Delta x$
0.01	3.93	4.65	4.85	5.76
0.1	3.93	4.68	4.85	5.76
0.5	3.89	5.26	4.85	5.76
0.7	3.90	9.64	4.85	5.76
0.9	4.01	10.75	4.85	5.77
1.0	4.15	11.23	4.85	5.77
1.5	5.95	13.28	4.94	5.80
1.9	7.27	14.50	5.63	6.57

Table 3
Number of points per wavelength for the space–time coupled approach using the RKo6s–CF8–CS6 combination.

ν	$\lambda_p^\phi/\Delta x$	$\lambda_a^\phi/\Delta x$	$\lambda_p^E/\Delta x$	$\lambda_a^E/\Delta x$
0.01	5.42	7.45	4.21	5.66
0.1	5.42	7.42	4.21	5.66
0.5	5.31	6.86	4.22	5.67
0.7	5.27	6.54	4.22	5.68
0.9	5.28	6.38	4.22	5.69
1.0	5.33	6.39	4.22	5.70
1.5	6.20	11.84	4.61	5.77
1.9	7.38	12.96	5.61	6.66

For the coupled space–time analysis, the results may now depend on the CFL number ν. The results obtained for the considered schemes are summarized in Table 2 and Table 3. It can be found that, when the CFL number ν tends to 0, the relative error on dispersion and dissipation due to the time integration procedure decreases and the (standard) results for the (standard) spatial spectral analysis are obviously recovered. In terms of dispersion, the required number of points per wavelength does not necessary increase when the CFL number ν increases since the dispersion curves are non-monotonic. In contrast, in terms of dissipation, the required number of points per wavelength increases when the CFL number ν increases.

2.6. Summary

It has been shown that the time integration procedure has an effect on the spectral behaviour of the scheme. Of course, standard results are recovered when the CFL number tends to 0. For the CS6 compact scheme, accounting for the time integration procedure does not really change the required number of points per wavelength up to $\nu = 1$. However, the situation differs for the DRP scheme FDo11p since the number of points per wavelength must be increased. Both filters CF8 and SFo11p are not specifically sensitive to the CFL number ν up to $\nu = 1$. As a consequence, this analysis shows that the coupled space–time approach is a prerequisite to deduce the number of grid points per wavelength.

Moreover, a general method to study the spectral behaviour of space–time discretisation has been recalled. As shown next in Sec. 3, such a coupled approach is mandatory to describe the spectral behaviour of spectral discontinuous techniques.

3. Spectral analysis of the spectral difference method

This section is devoted to the Fourier analysis of the SD method. As before, the analysis is performed on the advection equation (1).

3.1. Description of the spectral difference method

The spectral difference method solves in any cell the strong form of the equation per direction, as in the FD approach. The concept of the SD approach is simple: if the solution u evolves as a polynomial of degree p, the divergence of the flux must also be a polynomial of degree p and therefore the flux polynomial must be a polynomial of degree $p + 1$. Instead of defining any polynomial by its monomial coefficients, polynomials are defined by their values on a set of points and by Lagrange interpolation. We introduce the set of $p + 1$ points called *solution points* denoted as $(SP_l)_{1 \leq l \leq p+1}$ and the $p + 2$ points called *flux points* denoted as $(FP_l)_{1 \leq l \leq p+2}$. Let $\mathcal{L}_l$ (respectively $\mathcal{T}_l$) be the Lagrange polynomials of degree p (resp. $p + 1$) based on the solution (resp. flux) point index l. Details regarding the procedure to compute the flux divergence are given in Appendix B.

3.2. Matrix form of the SD procedure

Since the polynomials are defined on a Lagrange basis, any polynomial is defined by its values at the control points (either solution points or flux points). We introduce $\overline{\mathbf{U}}_i(t)$, the column vector of size $p+1$ (whose components are the solutions at solution points) as:

$$\overline{\mathbf{U}}_i(t) = [u_i(SP_l, t)]_{1 \leqslant l \leqslant p+1}^{\top}, \tag{11}$$

where $^{\top}$ means the transpose operation.

The first step is the extrapolation of the solution at the flux points using the form of polynomials, leading to the column vector $\overline{\mathbf{V}}_i(t)$ of size $p+2$ defined by:

$$\overline{\mathbf{V}}_i(t) = [u_i(FP_l, t)]_{1 \leqslant l \leqslant p+2}^{\top} = \left[\sum_{r=1}^{p+1} u_i(SP_r, t) \mathcal{L}_r(FP_l) \right]_{1 \leqslant l \leqslant p+2}^{\top}. \tag{12}$$

Since a Riemann problem must be solved on the cell boundaries, informations from neighbouring cells $i-1$ and $i+1$ are required. Solutions at solution points $\widetilde{\mathbf{U}}_i(t)$ and solutions at flux points $\widetilde{\mathbf{V}}_i(t)$ including solutions on the border flux points from adjacent cells are now defined as column vectors of size $3 \times (p+1)$ and $p+4$, respectively:

$$\widetilde{\mathbf{U}}_i(t) = \begin{bmatrix} \overline{\mathbf{U}}_{i-1}(t) \\ \overline{\mathbf{U}}_i(t) \\ \overline{\mathbf{U}}_{i+1}(t) \end{bmatrix}, \tag{13}$$

$$\widetilde{\mathbf{V}}_i(t) = \begin{bmatrix} u_{i-1}(FP_{p+2}, t) \\ \overline{\mathbf{V}}_i(t) \\ u_{i+1}(FP_1, t) \end{bmatrix}. \tag{14}$$

Defining $O_{m,n}$ as the zero matrix of dimension $m \times n$ and I_n the identity matrix of size n, the extrapolation matrix E of size $(p+4) \times (3 \times (p+1))$ such that $\widetilde{\mathbf{V}}_i(t) = E\widetilde{\mathbf{U}}_i(t)$ reads as:

$$E = \begin{bmatrix} [\mathcal{L}_l(FP_{p+2})]_{1 \leqslant l \leqslant p+1} & O_{1,p+1} & O_{1,p+1} \\ O_{1,p+1} & [\mathcal{L}_l(FP_1)]_{1 \leqslant l \leqslant p+1} & O_{1,p+1} \\ O_{1,p+1} & [\mathcal{L}_l(FP_2)]_{1 \leqslant l \leqslant p+1} & O_{1,p+1} \\ \vdots & \vdots & \vdots \\ O_{1,p+1} & [\mathcal{L}_l(FP_{p+2})]_{1 \leqslant l \leqslant p+1} & O_{1,p+1} \\ O_{1,p+1} & O_{1,p+1} & [\mathcal{L}_l(FP_1)]_{1 \leqslant l \leqslant p+1} \end{bmatrix}. \tag{15}$$

The second step consists of computing the flux. Here, the Riemann problem is solved using the (upwind) Godunov scheme:

$$\mathcal{F}_{Riemann}(u_L, u_R) = c\left(\frac{1 + sign(c)}{2} u_L + \frac{1 - sign(c)}{2} u_R \right), \tag{16}$$

where $sign(c) = c/|c|$. The computation of the flux at the flux points can be defined by the matrix F of size $(p+2) \times (p+4)$:

$$F = c \begin{bmatrix} \dfrac{1+sign(c)}{2} & \dfrac{1-sign(c)}{2} & O_{1,p} & 0 & 0 \\ O_{p,1} & O_{p,1} & I_p & O_{p,1} & O_{p,1} \\ 0 & 0 & O_{1,p} & \dfrac{1+sign(c)}{2} & \dfrac{1-sign(c)}{2} \end{bmatrix}. \tag{17}$$

For the last step, the flux polynomial is differentiated and its divergence is computed at the solution points. The derivative matrix D of size $(p+1) \times (p+2)$ is then

$$D = \left[\mathcal{T}_l'(SP_r) \right]_{\substack{1 \leqslant r \leqslant p+1, \\ 1 \leqslant l \leqslant p+2.}}$$

The overall process for computing the divergence term from the solution points can now be written in the following compact matrix form as:

$$M_1 = DFE, \tag{18}$$

with M_1 a matrix of size $(p+1) \times (3(p+1))$.

Table 4
CFL stability bounds for the SD method with Runge–Kutta time integration (RKo6s).

p	ν	$\hat{\nu}$
2	0.542304	1.626913
3	0.337879	1.351515
4	0.233186	1.165928
5	0.172017	1.032102

3.3. Matrix form for the spectral analysis

The generating pattern for a one-dimensional problem is given by one cell, so let us introduce the discretised normal mode within this period $\overline{\mathbf{U}}_i(t) = \widehat{\mathbf{U}}_i(t)\exp(jik\Delta x)$ such that $\widetilde{\mathbf{U}}_i(t) = L\widehat{\mathbf{U}}_i(t)$. Introducing the complex-valued matrix L of size $3(p+1) \times (p+1)$:

$$L = \begin{bmatrix} \exp(-jk\Delta x)\,I_{p+1} \\ I_{p+1} \\ \exp(jk\Delta x)\,I_{p+1} \end{bmatrix}, \tag{19}$$

it comes easily:

$$\frac{\partial \widehat{\mathbf{U}}_i(t)}{\partial t} = M\widehat{\mathbf{U}}_i(t), \tag{20}$$

where $M = -DFEL = -M_1 L$.

3.4. Time discretisation

Eq. (20) is a system of linear differential equations whose integration is carried out using the low-storage second-order six-stage Runge–Kutta scheme of Bogey and Bailly [31], as in Sec. 2. $\widehat{\mathbf{U}}_i(t)$ is discretised by $\widehat{\mathbf{U}}_i^n = \widehat{\mathbf{U}}_i(n\Delta t)$ and the discrete solution is advanced in time using

$$\widehat{\mathbf{U}}_i^{n+1} = \left[I_{p+1} + \sum_{l=1}^{6} \gamma_l \Delta t^l M^l \right] \widehat{\mathbf{U}}_i^n = G\widehat{\mathbf{U}}_i^n. \tag{21}$$

G is a square complex-valued matrix of size $p+1$ which accounts for both space and time integration. G depends on the polynomial degree p, on the wavenumber k and of course on the CFL number $\nu = c\Delta t/\Delta x$. It is important to note that we keep here the standard definition of the CFL number for an advection equation.

3.5. Stability analysis based on CFL criterion

The SD method with the Runge–Kutta time integration is stable under a CFL condition, similarly as the FD method. Starting from Eq. (21), the matrix geometric progression between $\widehat{\mathbf{U}}_i^{n+1}$ and $\widehat{\mathbf{U}}_i^n$ is convergent if the spectral radius ρ of matrix G is strictly lower than 1. The stability limits found are summarized in Table 4. To be able to compare with the FD method, let us define a new CFL number as $\widehat{\nu} = (c\Delta t/\Delta x)(p+1) = \nu(p+1)$ with a length scale which corresponds to the mean distance between two adjacent degrees of freedom.

3.6. Application of the Nyquist–Shannon sampling theorem

The Nyquist–Shannon sampling theorem states that at least two points are mandatory to capture a given frequency. Such an approach is routinely applied in standard schemes such as FD. Here, let us consider a vector $\widehat{\mathbf{U}}_i^n$ sampled over a cell of size Δx. The sampling frequency f_s is therefore $f_s = 1/\Delta x$. It is assumed that the vector $\overline{\mathbf{U}}_i$ represents the normal mode as in Sec. 3.3:

$$\overline{\mathbf{U}}_i(t,k) = \widehat{\mathbf{U}}_i(t)\exp(jik\Delta x). \tag{22}$$

Computing now the same kind of relation for a new normal mode with $k' = k + m(2\pi/\Delta x) = k + m(2\pi f_s)$ ($m \in \mathbb{Z}$), one finds:

$$\overline{\mathbf{U}}_i(t,k') = \widehat{\mathbf{U}}_i(t)\exp(jik'\Delta x),$$
$$= \widehat{\mathbf{U}}_i(t)\exp(ji(k + 2m\pi/\Delta x)\Delta x),$$
$$= \widehat{\mathbf{U}}_i(t)\exp(jik\Delta x + ij2m\pi),$$
$$= \overline{\mathbf{U}}_i(t,k),$$

because $im \in \mathbb{Z}$. As a consequence, any normal mode $\overline{\mathbf{U}}_i(t, k + 2m\pi/\Delta x)$ with $m \in \mathbb{Z}$ has the *same representation* after sampling at the solution points and we note that, in order to avoid aliasing, $k\Delta x$ should belong to $[0, \pi]$. This is a key point and in all previous studies on spectral accuracy (for DG, SD, SV and FR), such a property was always lost [20,25–30]. An illustration of the aliasing phenomenon for $k\Delta x > \pi$ will be shown in Sec. 4.

3.7. Matrix power method for the spectral analysis

Eq. (21) introduces the transfer matrix G between time steps n and $n + 1$:

$$\widehat{\mathbf{U}}_i^{n+1} = G\widehat{\mathbf{U}}_i^n. \tag{23}$$

and using properties of geometric progressions and Eq. (23), one obtains, raising G to the power n:

$$\widehat{\mathbf{U}}_i^n = G^n\widehat{\mathbf{U}}_i^0. \tag{24}$$

Carrying out an unsteady computation (for the advection equation) with the Spectral Difference method simply consists of computing the n-th power of the matrix G in order to obtain the solution at the n-th time iteration from the initial solution. The computation of the n-th power of any matrix is at the core of the Matrix Power Method (MPM) also called Power Iteration or Power Method [39,40]. The main properties of the MPM are summarized below for completeness.

The MPM gives a well-known algorithm for the computation of the spectral radius of a matrix, *i.e.* the eigenvalue with the largest modulus. The proof of the theorem can be found in [39] and it is introduced hereafter since it enables to establish a general result for the spectral analysis of the SD Method. [R3:] *Since Eq. (23) is the expression of a matrix geometric progression, its behaviour is given by the eigenvalue with the largest modulus when n tends to infinity because among all the modes, the considered one has the least dissipation. This is the reason why, even if all the eigenvalues were computed, only the one with the largest modulus was retained according to the MPM.*

3.7.1. The matrix power method for SD

G is a $(p + 1) \times (p + 1)$ matrix with complex coefficients. Consider the eigenvalue problem $G\widehat{\mathbf{U}}_i = \lambda\widehat{\mathbf{U}}_i$, where $\widehat{\mathbf{U}}_i \neq 0$, $\widehat{\mathbf{U}}_i \in \mathbb{C}^{(p+1)\times 1}$ and $\lambda \in \mathbb{C}$. $\widehat{\mathbf{U}}_i$ is indeed a column vector.

Assumptions. We assume that the eigenvalue problem $G\mathbf{v}_l = \lambda_l\mathbf{v}_l$ with $\lambda_l \in \mathbb{C}$ and $\mathbf{v}_l \in \mathbb{C}^{(p+1)\times 1}$ admits a complete normalized eigenvector space $(\mathbf{v}_1, \mathbf{v}_2, ..., \mathbf{v}_{p+1})$ spanning $\mathbb{C}^{(p+1)}$ with corresponding eigenvalues satisfying $|\lambda_1| < |\lambda_l|$, $l \neq 1$ and $|\lambda_l| < |\lambda_{p+1}|$, $l \neq p + 1$.

From now on, let the initial condition $\widehat{\mathbf{U}}_i^0$ be a given vector, for which

$$\widehat{\mathbf{U}}_i^0 = \sum_{l=1}^{p+1}\alpha_l^{(0)}\mathbf{v}_l, \text{ with } \alpha_{p+1}^{(0)} \neq 0, \tag{25}$$

and let

$$\forall n \in \{1, 2, ...\}, \ \widehat{\mathbf{U}}_i^n = G\widehat{\mathbf{U}}_i^{n-1}, \tag{26}$$

be the basic recursive sequence. From Eq. (25) and Eq. (26), it comes immediately:

$$\widehat{\mathbf{U}}_i^n = \sum_{l=1}^{p+1}\alpha_l^{(0)}G^n\mathbf{v}_l.$$

Furthermore, $G^n\mathbf{v}_l = \lambda_l^n\mathbf{v}_l$, for all $l \in \{1, 2, ..., p + 1\}$, and as a consequence:

$$\widehat{\mathbf{U}}_i^n = \sum_{l=1}^{p+1}\alpha_l^{(0)}\lambda_l^n\mathbf{v}_l$$

or equivalently:

$$\widehat{\mathbf{U}}_i^n = \alpha_{p+1}^{(0)}\lambda_{p+1}^n\left(\mathbf{v}_{p+1} + \sum_{l=1}^{p}\frac{\alpha_l^{(0)}}{\alpha_{p+1}^{(0)}}\left(\frac{\lambda_l}{\lambda_{p+1}}\right)^n\mathbf{v}_l\right).$$

Hence, using $\left|\frac{\lambda_l}{\lambda_{p+1}}\right| = 1 - \frac{|\lambda_{p+1}| - |\lambda_l|}{|\lambda_{p+1}|}$, it comes:
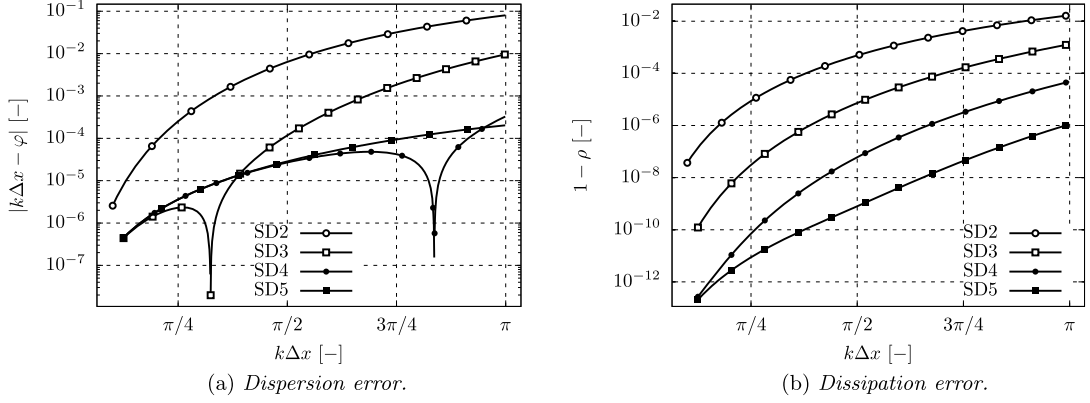
Fig. 3. Spectral analysis for the RKo6s–SD schemes with CFL condition $\nu = 0.1$: effect of the order of the solution reconstruction.

$$\left\| \mathbf{v}_{p+1} - \frac{1}{\alpha_{p+1}^{(0)} \lambda_{p+1}^n} \widehat{\mathbf{U}}_i^n \right\|_\infty \leqslant \sum_{l=1}^{p} \left| \frac{\alpha_l^{(0)}}{\alpha_{p+1}^{(0)}} \right| \left(1 - a_{p+1} \right)^n, \tag{27}$$

where

$$a_{p+1} = \min_{\substack{l \in \{1,\dots,p\} \\ l \neq p+1}} \left| \frac{\left| \lambda_{p+1} \right| - |\lambda_l|}{\lambda_{p+1}} \right|.$$

Noticing that

$$\lim_{n \to +\infty} \left(1 - a_{p+1} \right)^n = 0,$$

one can easily deduce from Eq. (27) that

$$\widehat{\mathbf{U}}_i^n \underset{n \to +\infty}{\sim} \alpha_{p+1}^{(0)} \lambda_{p+1}^n \mathbf{v}_{p+1}. \tag{28}$$

So, $\widehat{\mathbf{U}}_i^n$ behaves as $\alpha_{p+1}^{(0)} \lambda_{p+1}^n \mathbf{v}_{p+1}$ when the number of iterations of the time integration n is large. Moreover, the difference between the true behaviour and its asymptotic approximation depends on how the ratios $\left| \lambda_l / \lambda_{p+1} \right|$ for $l \in \{1, \dots, p\}$ decay to 0. For a large number of iterations and for any guess $\widehat{U}_i^0$ with $\alpha_{p+1}^{(0)} \neq 0$, $\widehat{U}_i^n$ behaves in the direction of the dominant eigenvector $\mathbf{v}_{p+1}$.

3.7.2. Results of the MPM for SD

The Matrix Power Method gives a way to perform the spectral analysis of the Spectral Difference method. The dispersion and the amplification are simply given by the spectral radius $|\lambda_{p+1}|$ of the matrix G. Between the iterations n and $n + 1$, the dispersion is given by the argument $\varphi = -\arg\left(\lambda_{p+1} \right) / \nu$ and the amplification is given by $\rho = \left| \lambda_{p+1} \right|$.

Remark. In all the cases presented in this paper, we found numerically that the eigenvalue problem $G\mathbf{v}_l = \lambda_l \mathbf{v}_l$ always satisfied the assumptions given above. We did not succeed in demonstrating mathematically such a result for any value of the polynomial degree p. This is left as a future line of research.

Remark. It should be noted that the Matrix Power Method can be applied to any kind of high-order spectral discontinuous method, since the discrete space–time integration can be written in the form of Eq. (26) for an advection equation.

3.8. Comparison with numerical results

Numerical solutions in 1D are now computed to support the theoretical results on dispersion and dissipation in Figs. 3a and 3b. The advection equation Eq. (1) with $c = 1.0$ [m/s] is solved using the Spectral Difference method previously mentioned with $\nu = 0.1$. The initial solution is $u_0(x) = \sin(kx)$. The one-dimensional mesh is composed of 40 regular cells with a cell length $\Delta x = 2.0$. The system is closed with periodic boundary conditions. Indeed, numerical computations are performed with $k\Delta x = 0.1\pi n$ with $n \in \mathbb{N}$, $1 \leqslant n \leqslant 9$ for $p = 2$ and $2 \leqslant n \leqslant 9$ for $p = 3$ and $p = 4$. One obtains $2n$ periods on this specific mesh.

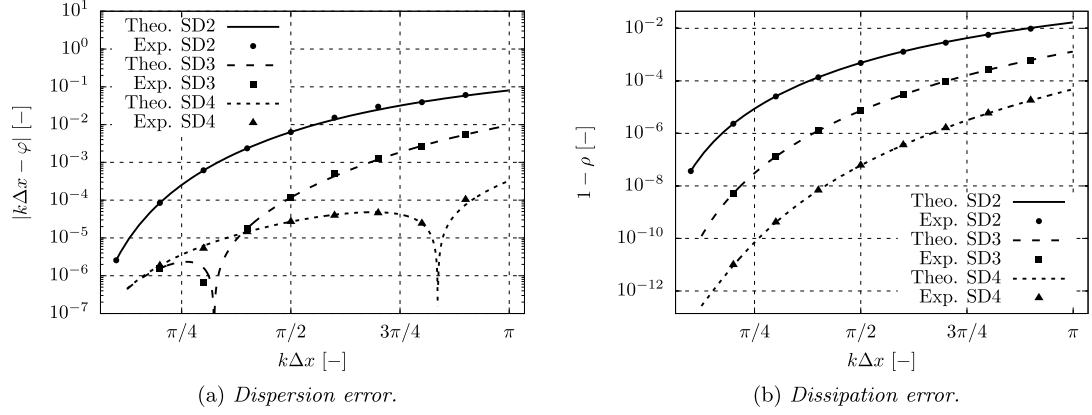(a) *Dispersion error.*　　(b) *Dissipation error.*

Fig. 4. Spectral analysis for t he RKo6s-SD schemes with CFL condition $\nu = 0.1$: comparison of theoretical spectral behaviours with numerical solutions and effect of different polynomial orders.
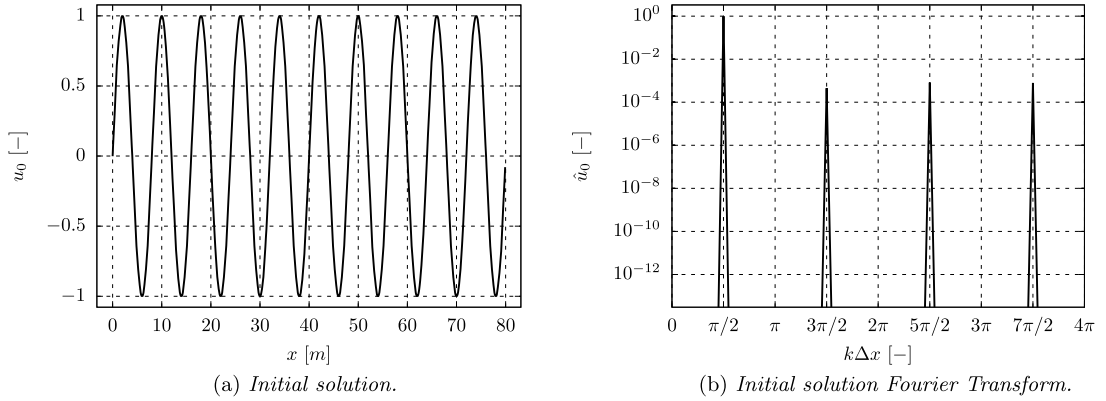

(a) *Initial solution.*　　(b) *Initial solution Fourier Transform.*

Fig. 5. Initial solution for $k\triangle x = \pi/2$.

The initial solution is transported over a sufficient number of discrete time instants to measure the dissipation and the dispersion. The amplification and the phase shift are identified by a minimization process using the least squares method to solve:

$$\min_{\substack{A\in\mathbb{R}^{+*} \\ \phi\in[0,2\pi[}} ||f(x,t) - A\sin(kx + \phi)||_2 , \tag{29}$$

where $\| \cdot \|_2$ is the standard L^2 norm for functions. It is shown in Fig. 4a and Fig. 4b that theoretical and numerical behaviours for dispersion and dissipation are in a very good agreement, for $p = 2$, $p = 3$ and $p = 4$ respectively.

## 4. Extension to high wavenumbers for the spectral difference method

It was shown in Sec. 3.6 that the standard spectral analysis, with Fourier modes, cannot be applied to wavenumbers greater than π. This is a consequence of the Nyquist–Shannon sampling theorem. However, the spectral analysis published in the literature allows to capture wavenumbers greater than π [25–29,20,30]. This section is devoted to the analysis of this phenomenon when the wavenumber is larger than π.

### 4.1. Aliasing and initial solution projection

In this section, we want to analyse the aliasing that occurs with high-order spectral methods. We consider as before an advection equation problem with periodic conditions. For a given $\triangle x$, two simulations are performed. For the first one, the wavenumber k is chosen such that $k\triangle x = \pi/2$, while for the second case, the wavenumber k is such that $k\triangle x = 3\pi/2$. For both cases, we select $p = 3$.

For the first computation, the initial, final solutions, and their corresponding Fourier transform, are shown in Fig. 5 and Fig. 6. The solution is almost conserved and the energy repartition per mode does not change significantly.

Regarding the second case with $k\triangle x = 3\pi/2$, the initial solution and the associated Fourier spectrum are shown in Fig. 7. After many iterations (we do not define the number of iterations here since it is the topic of Sec. 4.3 and Sec. 4.4), the final
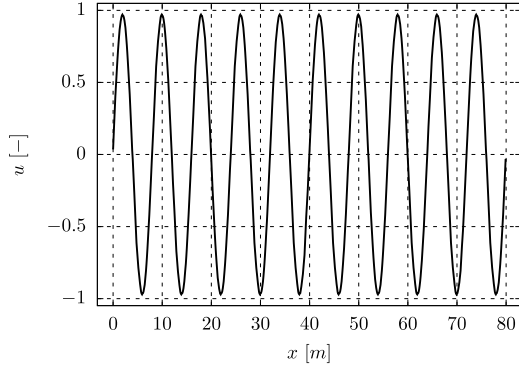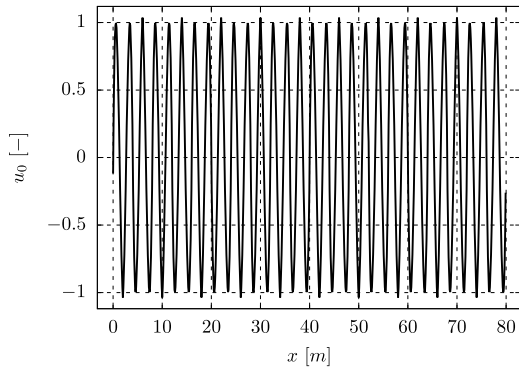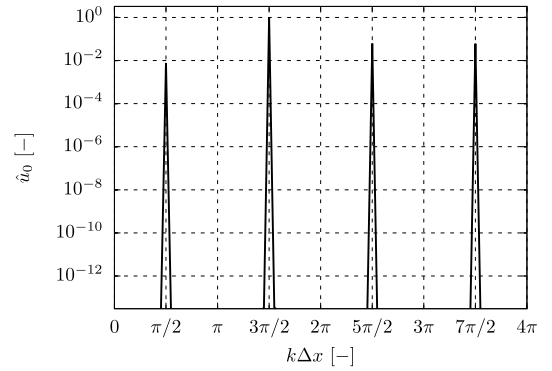
(a) *Final solution.*
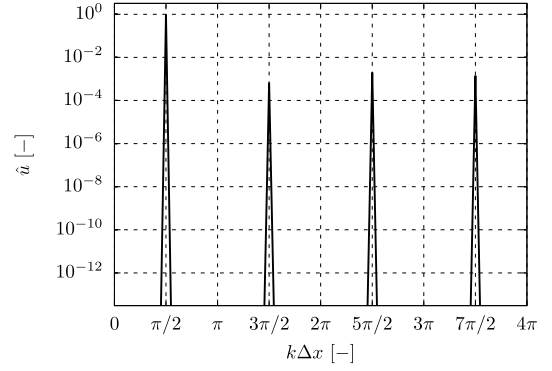
(b) *Final solution Fourier Transform.*
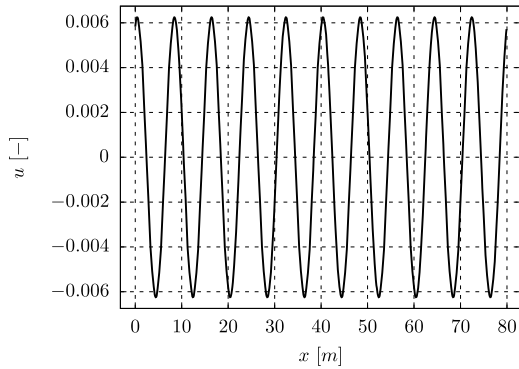
Fig. 6. Final solution for $k\Delta x = \pi/2$.
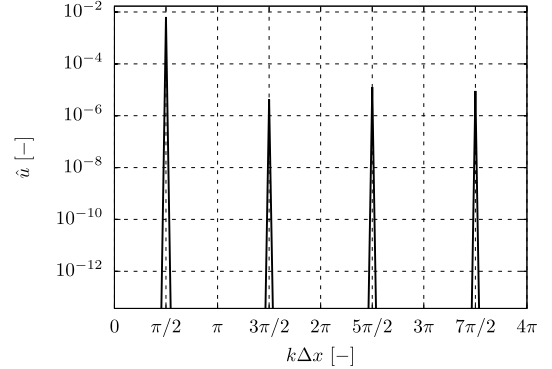

(a) *Initial solution.*

(b) *Initial solution Fourier Transform.*

Fig. 7. Initial solution for $k\Delta x = 3\pi/2$.

(a) *Final solution.*

(b) *Final solution Fourier Transform.*

Fig. 8. Final solution for $k\Delta x = 3\pi/2$.

solution and the associated spectrum are shown in Fig. 8. We remark that the mode $k\Delta x = \pi/2$ now contains the largest part of the energy, while the mode $k\Delta x = 3\pi/2$ initially had the largest energy. All modes larger than π are damped and it remains essentially the mode associated with $k\Delta x = \pi/2$.

This numerical experiment points out the aliasing phenomenon revealed by our analysis. Such aliasing occurs for any value of p, but the time to see an effect varies with p, the number of iterations, the CFL number and the wavenumber one looks for. Moreover, the standard Fourier spectral analysis can only be applied once the initial wavenumber is unchanged: dissipation and dispersion are defined for a given frequency. Here, since the frequency (with the main part of the energy) changes, it is mandatory to introduce a new way to estimate dissipation and dispersion. In the following, dissipation is expressed using relations defined with energy preserving relations, while dispersion is obtained from a scalar product.

4.2. Mathematical consideration

Let us define the space $L^2([-1, +1])$ of complex-valued functions on the closed interval $[-1, +1]$ and the associated complex scalar product by:

$$\forall (f, g) \in \left(L^2([-1, +1])\right)^2, \quad \langle f, g \rangle = \int_{-1}^{+1} f(x) \times \mathrm{conj}(g)(x)\,dx, \tag{30}$$

where $\mathrm{conj}(g)$ is the complex conjugate of g. Obviously, the norm associated with this scalar product is defined by:

$$\forall f \in L^2([-1, +1]), \quad \|f\| = \sqrt{\int_{-1}^{+1} |f(x)|^2\,dx}. \tag{31}$$

Moreover, $\|\alpha e^{j\beta} f\| = \alpha \|f\|$ and $\langle \alpha e^{j\beta} f, g \rangle = \alpha e^{j\beta} \langle f, g \rangle$ for all $(\alpha, \beta) \in \mathbb{R}^+ \times [0, 2\pi[$ by sesquilinearity of the complex scalar product.

Let us use this complex scalar product to compute the dispersion and the dissipation of the Spectral Difference method. For wavenumbers in $[0, \pi]$, the spectral analysis follows the MPM. However, for wavenumbers larger than π, coming back to the physical meaning of dissipation and dispersion, *dissipation can be expressed as the rate of loss in energy of the signal, while dispersion is the phase shift of the signal*. In the case of spectral analysis, the functions f are simply represented by the complex exponential basis $f^n(x) = \exp(-j\omega n \Delta t + jkx) = \alpha e^{j\beta} f^0(x)$. The dissipation and the dispersion after n iterations can be expressed as the product of the initial solution by $\alpha e^{j\beta}$. Mathematically, the dissipation is defined as the loss of the L^2-norm of the signal f between time 0 and n by:

$$\frac{\|f^n\|}{\|f^0\|} = \frac{\|\alpha e^{j\beta} f^0\|}{\|f^0\|} = \alpha. \tag{32}$$

The phase shift of the signal f between time 0 and n can be simply expressed as:

$$\arg\left(\langle f^n, f^0 \rangle\right) = \arg\left(\langle \alpha e^{j\beta} f^0, f^0 \rangle\right) = \arg\left(\alpha e^{j\beta} \langle f^0, f^0 \rangle\right) = \arg\left(\alpha e^{j\beta} \|f^0\|^2\right) = \beta. \tag{33}$$

The complex scalar product is defined on $L^2([-1, +1])$ and this is the right way to take into account the fact that all quantities are defined by polynomials. However, Eq. (32) and Eq. (33) are obtained using only the sesquilinearity of the complex scalar product since the definition of the scalar product (Eq. (30)) is never explicitly used. Actually, the definition of both dispersion and dissipation does not depend on the considered scalar product. It is more convenient (and simple!) to replace the L^2 norm for functions by the ℓ^2-norm $\|\cdot\|_2$ of vectors in $\mathbb{C}^{p+1}$, playing directly with the solutions at solution points. Of course, this norm is derived from the following complex scalar product:

$$\forall (x, y) \in \left(\mathbb{C}^{p+1}\right)^2, \quad \langle x, y \rangle = \sum_{l=1}^{p+1} x_l \times \mathrm{conj}(y_l). \tag{34}$$

4.3. Energy loss estimation

As explained before, we replace the standard L^2-norm of functions by the ℓ^2-norm of the solution point vectors $\widehat{U}_i^n$. Let us introduce the ratio $\rho_{n,m}$ for $(n, m) \in \mathbb{N}^+ \times \mathbb{N}^+$ with $n > m$:

$$\rho_{n,m} = \frac{\|\widehat{U}_i^n\|_2}{\|\widehat{U}_i^{n-m}\|_2}. \tag{35}$$

By definition, $\rho_{n,m}$ represents the energy loss of the solution between iteration $n - m$ ($n \geq m$) and iteration n. The MPM gives the behaviour of $\rho_{n,m}$ when n is sufficiently large:

$$\rho_{n,m} = \sqrt{\frac{\sum_{l=1}^{p+1} \left|\alpha_l^{(0)} \lambda_l^n\right|^2}{\sum_{l=1}^{p+1} \left|\alpha_l^{(0)} \lambda_l^{n-m}\right|^2}} \underset{n \to +\infty}{\sim} \left|\lambda_{p+1}^m\right| \underset{n \to +\infty}{\sim} \rho^m. \tag{36}$$

Using Eq. (36), it is clear that $\rho_{n,m}$ is a generalization of the standard criterion for scheme dissipation and $\rho_{n,m}$ behaves as the spectral radius raised to a power equal to the number of iterations.
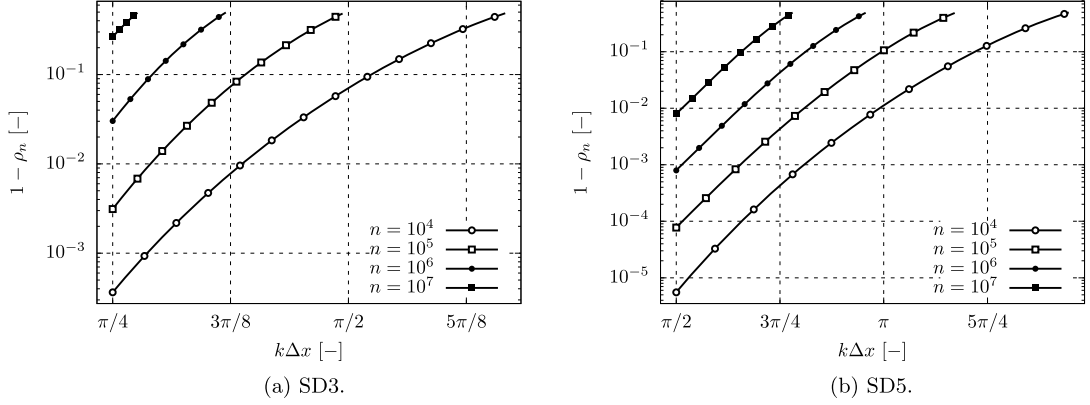
Fig. 9. Loss in energy for two values of p as a function of the number of iterations ($\nu = 0.1$).

Let $\rho_n = \rho_{n,n}$ represent an estimation of the energy loss by the initial signal after n iterations. In Fig. 9, the loss in energy for two values of p is shown as a function of the number of iterations for computations performed at CFL number $\nu = 0.1$. As expected, the loss in energy increases with the number of iterations to perform. ρ_n measures the dissipation effect above π but we need to introduce a new quantity to account for dispersion.

4.4. Phase shift estimation

Let us introduce $\delta\varphi_{n,m}$ for $(n,m) \in \mathbb{N}^+ \times \mathbb{N}^+$ with $n > m$:

$$\delta\varphi_{n,m} = \arg\left(\langle \widehat{U}_i^n, \widehat{U}_i^{n-m} \exp\left(-jm\nu k\Delta x\right)\rangle\right). \tag{37}$$

$\delta\varphi_{n,m}$ represents the phase shift of the solution between iterations $n - m$ and n. Indeed, the factor $\exp\left(-jm\nu k\Delta x\right)$ takes into account the theoretical advection given by the analytical solution of the advection equation with a constant advective velocity c. We have:

$$\delta\varphi_{n,m} \underset{n\to+\infty}{\sim} \arg\left(\alpha_{p+1}^{(0)}\lambda_{p+1}^n \mathrm{conj}(\alpha_{p+1}^{(0)}\lambda_{p+1}^{n-m}) \exp\left(jm\nu k\Delta x\right)\right) \tag{38}$$

$$\underset{n\to+\infty}{\sim} \arg\left(\left|\alpha_{p+1}^{(0)}\right|^2 \rho^n \exp\left(-jn\nu\varphi\right)\rho^{n-m} \exp\left(j\left(n-m\right)\nu\varphi\right)\exp\left(jm\nu k\Delta x\right)\right) \tag{39}$$

$$\underset{n\to+\infty}{\sim} \arg\left(\rho^{2n-m}\left|\alpha_{p+1}^{(0)}\right|^2 \exp\left(jm\nu\left(k\Delta x - \varphi\right)\right)\right) \tag{40}$$

$$\underset{n\to+\infty}{\sim} m\nu\left(k\Delta x - \varphi\right). \tag{41}$$

This criterion computes the phase shift of the signal induced by the numerical scheme between iteration n and iteration $n - m$. Let us note $\delta\varphi_{n,n} = \delta\varphi_n$ which computes an estimation of the phase delay between the signal after n iterations and the initial signal which has been analytically convected. It measures the overall dispersion induced by the time integration loop. This latter is a generalization of the usual criterion but it takes into account the effect of the time integration. Indeed, the spectral behaviour evolves during the number of iterations. Furthermore, $\delta\varphi_n/2\pi$ gives the phase shift length per number of wavelength. For example, $\delta\varphi_n/2\pi = 0.1$ means that both signals are separated by 0.1λ where λ is the signal wavelength. In Fig. 10, the phase shifts for SD3 and SD5 are shown as a function of the number of iterations, in a similar way as for Fig. 9.

4.5. Summary

In this section, new criteria for dissipation and dispersion have been introduced. The criteria take into account both space and time schemes. It is shown that for wavenumbers above π, aliasing occurs but the aliasing speed depends on the CFL number, the time integration procedure, the number of time steps and the polynomial degree p. The new criteria based on energy loss and phase shift are extensions of the standard Fourier approach introduced in the previous sections. In particular, the results presented in Sec. 3 are recovered by the new approach for wavenumbers in $[0, \pi]$ and a large number of iterations (asymptotic behaviour). We note that the new criteria are general in the sense that they can be applied to any kind of numerical scheme.

In the next section, these criteria are used to compare the Spectral Difference scheme with the Finite Difference approaches introduced in Sec. 2.
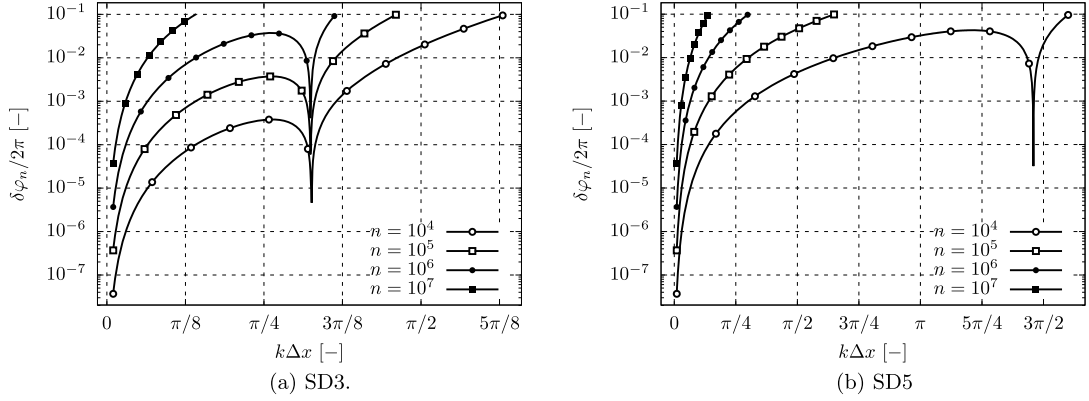
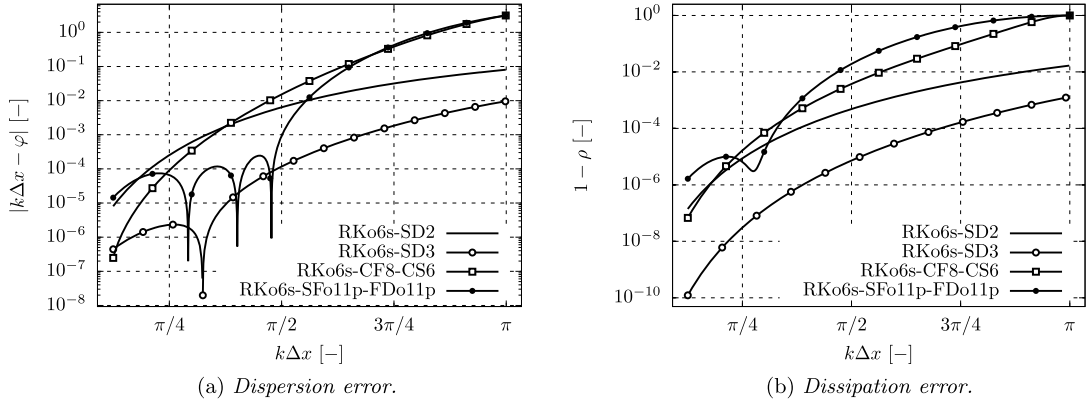**Fig. 10.** Phase shift for two values of p as a function of the number of iterations ($\nu = 0.1$).

Fig. 11. Spectral analysis for $\nu = 0.1$: comparison of the schemes. For SD schemes, these results are obviously those given by the MPM.

5. Comparison with standard high-order schemes

This section is devoted to the comparison of the spectral behaviour between the standard schemes for aeroacoutics and the Spectral Difference method.

5.1. Naive comparison

For standard spectral analysis of FD schemes, $\mathcal{G}(k\Delta x)$ defined in Eq. (8) can be seen as the transfer function between $\widehat{u}_i^n$ and $\widehat{u}_i^{n+1}$ after applying the spatial numerical scheme, the time integration and the filter. Like all transfer functions, it can be characterised by its modulus, which was called $\rho = |\mathcal{G}|$, and its argument, which was called $\varphi = -\arg(\mathcal{G})/\nu$. Note that the argument of $\mathcal{G}(k\Delta x)$ was (i) multiplied by (-1) because of the normal mode choice $u_i^n = \exp((-1)jn\omega\Delta t + jik\Delta x)$ and (ii) divided by the CFL number ν to obtain a quantity which is always equal to $k\Delta x$ in the exact case since the dimensionless dispersion relation is $\omega\Delta t = \nu k\Delta x$. For the spectral analysis of the Spectral Difference method, the transfer function is λ_{p+1}. Indeed, when the number of iterations is large, $\widehat{U}_i^{n+1}$ is obtained from $\widehat{U}_i^n$ multiplied by λ_{p+1}. Analogously, $\varphi = -\arg(\lambda_{p+1})/\nu$ and $\rho = |\lambda_{p+1}|$ were defined. These quantities are plotted in Fig. 11a and Fig. 11b respectively.

In the light of these figures, the RKo6s–SD2 scheme seems to have a similar spectral behaviour as both RKo6s–CF8–CS6 and RKo6s–SFo11p–FDo11p. Nevertheless one has to remember that several degrees of freedom are located within any mesh element in the Spectral Difference approach. It is therefore preferable to introduce a new criterion that takes into account the total number of degrees of freedom instead of the number of mesh elements and their size.

5.2. Rescaling by the number of degrees of freedom

For a fair comparison, the analysis may be performed considering the dimensionless wavenumber $k\Delta x'$ built with the mean distance between two degrees of freedom and not with the element size Δx. It means that, for the Spectral Difference method, the dimensionless wavenumber should be $k\Delta x/(p+1)$ whereas, for standard schemes, the dimensionless wavenumber remains $k\Delta x$. Of course, the same rescaling is performed for the CFL number: $\widehat{\nu} = (p+1)c\Delta t/\Delta x$ for the SD method while $\nu = c\Delta t/\Delta x$ for FD schemes. Dispersion and dissipation are now defined as a function of the number of
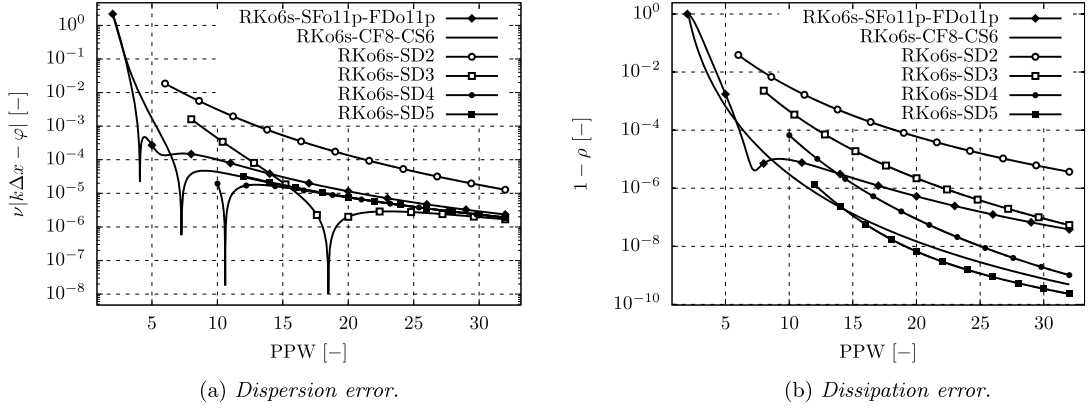
(a) *Dispersion error.* (b) *Dissipation error.*

Fig. 12. Spectral analysis for $\nu = 0.7$: comparison of the considered schemes.

points per wavelength (PPW) and two definitions are introduced: $PPW = (p+1)\lambda/\Delta x$ for the Spectral Difference method while $PPW = \lambda/\Delta x$ for the FD schemes. Moreover, the CFL number is kept constant: $\widehat{\nu} = 0.7$ for SD method and $\nu = 0.7$ for standard schemes. This choice is motivated by the fact that both the SD and the finite difference methods lead to the same physical time step. Moreover, the CFL value is chosen in agreement with the one for previous aeroacoustic computations using the compact scheme.

Finally, it must be mentioned that the new quantity $\nu |k\Delta x - \varphi|$ is introduced to account for the change in CFL number definition for analysing dispersion.

In terms of dispersion, the RKo6s–SD4 method seems to be equivalent to the RKo6s–CF8–CS6 combination whereas in terms of dissipation, the RKo6s–CF8–CS6 combination is between the RKo6s–SD4 and RKo6s–SD5 method (Fig. 12). However, two problems can be observed. First, the dimensionless wavenumber belongs to $[0, \pi/(p+1)]$ for the SD method. So, it can not be compared on the full range of wavenumbers in $[0, \pi]$. Moreover, dispersion and dissipation in $[0, \pi/(p+1)]$ come from the asymptotic behaviour introduced in Sec. 3.7.2 and do not benefit from the matrix form of the SD method for wavenumbers higher than $\pi/(p+1)$. It is thus mandatory to extend the analysis in energy loss and phase shift to standard schemes for a fair comparison.

5.3. New criteria extension to standard aeroacoustic schemes

For the considered Finite Difference schemes with time integration and filtering, the solution is updated using a simple multiplication:

$$\widehat{u}_i^{n+1} = \mathcal{G}\widehat{u}_i^n \tag{42}$$

Introducing as before the loss in energy and the phase shift, it comes:

$$\rho_n = \frac{\|\widehat{u}_i^n\|_2}{\|\widehat{u}_i^0\|_2} = \frac{\|\mathcal{G}^n\widehat{u}_i^0\|_2}{\|\widehat{u}_i^0\|_2} = |\mathcal{G}|^n = \rho^n. \tag{43}$$

and

$$\delta\varphi_n = \arg\left(\widehat{u}_i^n \mathrm{conj}(\widehat{u}_i^0 \exp(-jn\nu k\Delta x))\right), \tag{44}$$

$$= \arg\left(\mathcal{G}^n\widehat{u}_i^0 \mathrm{conj}(\widehat{u}_i^0 \exp(-jn\nu k\Delta x))\right), \tag{45}$$

$$= \arg\left(\mathcal{G}^n \exp(jn\nu\, k\Delta x)\right), \tag{46}$$

$$= n\nu\, k\Delta x + n\arg(\mathcal{G}), \tag{47}$$

$$= n\nu\,(k\Delta x - \varphi). \tag{48}$$

Remark. The previous expressions are equalities and not asymptotic limits since $\mathcal{G}$ is a scalar quantity.
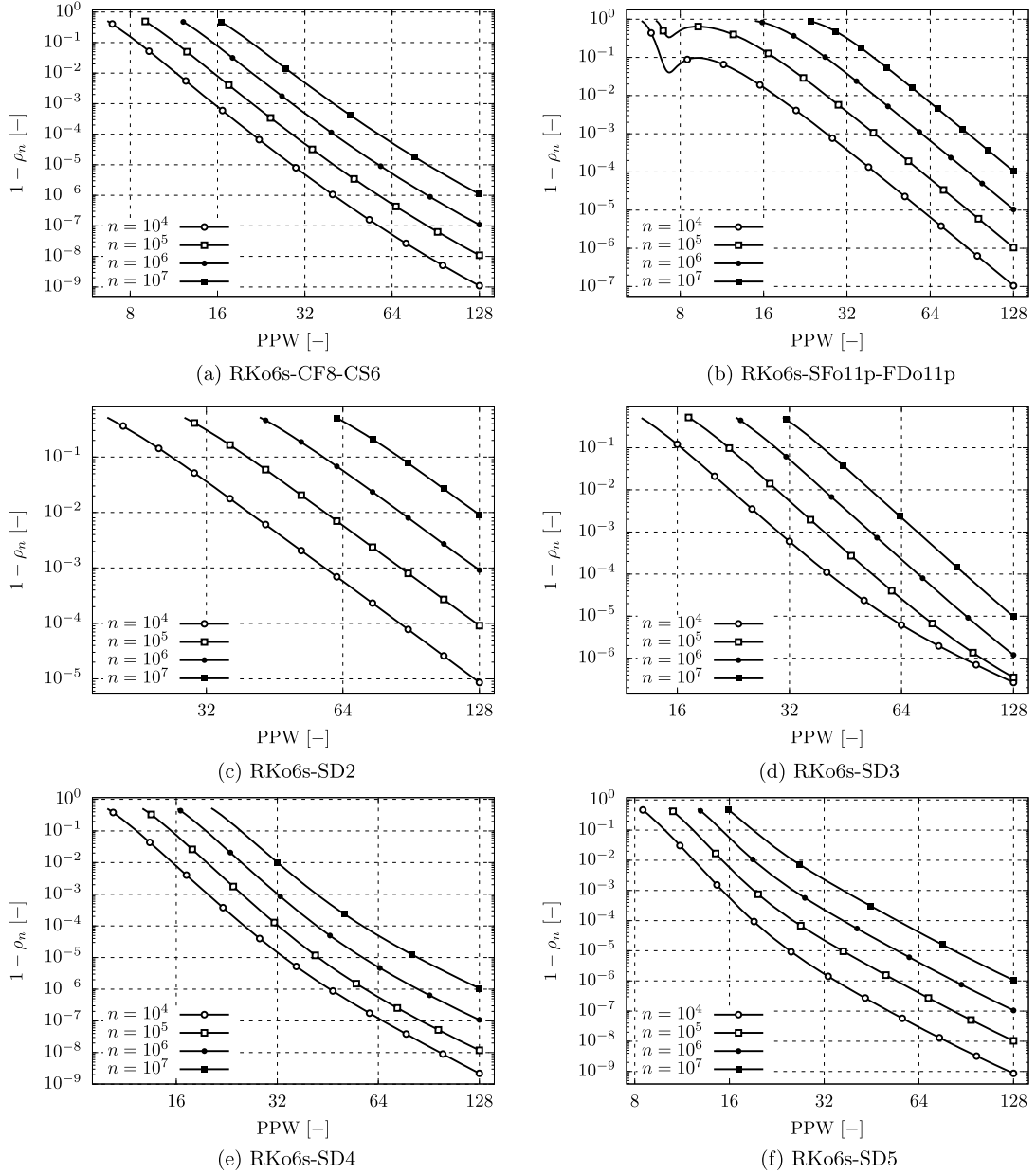
Fig. 13. Spectral analysis for $\nu = 0.7$: analysis of the dissipation-based criterion.

5.4. Points per wavelength (PPW) – dissipation-based criterion

Introducing the new criteria for Finite Difference schemes, it is now possible to define a cut-off wavenumber $k_c^{\varepsilon} \Delta x$ that is associated with the conservation of a certain percentage $1 - \varepsilon$ of energy after n iterations. To do so, it is mandatory to solve the following problem:

For a given set $(n, \nu, p) \in \left(\mathbb{N}^* \times \mathbb{R}^{+*} \times \mathbb{N}^* \right)$, look for

$$k\Delta x \in \left[0, k_c^{\varepsilon} \Delta x \right] \text{ such that } \rho_n\left(k\Delta x, n, \nu, p \right) \geqslant 1 - \varepsilon$$

This cut-off wavenumber can be obviously interpreted as a number of points per wavelength (PPW). The dissipation-based criteria is finally shown in Fig. 13 for both Finite Difference schemes, and for the Spectral Difference approach with p ranging from 2 to 5 and n from 10^4 to 10^7 at CFL number $\nu = 0.7$. The cases with $n = 10^4$ and $n = 10^5$ correspond to the typical numbers of iterations for standard LES. The extreme cases with $n > 10^5$ are only computed to illustrate the asymptotic behaviour.

Table 5
PPW for dissipation criterion $n = 10^4$.

	$\rho_{10^4} = 99.99\%$	$\rho_{10^4} = 99.9\%$	$\rho_{10^4} = 99\%$
RKo6s–SFo11p–FDo11p	40.30	27.03	17.67
RKo6s–CF8–CS6	21.08	15.54	11.52
RKo6s–SD2	85.51	58.38	39.74
RKo6s–SD3	40.87	29.89	22.17
RKo6s–SD4	25.52	19.86	15.59
RKo6s–SD5	19.01	15.18	12.32

Table 6
PPW for dissipation criterion $n = 10^5$.

	$\rho_{10^5} = 99.99\%$	$\rho_{10^5} = 99.9\%$	$\rho_{10^5} = 99\%$
RKo6s–SFo11p–FDo11p	59.55	40.29	27.00
RKo6s–CF8–CS6	28.89	21.07	15.53
RKo6s–SD2	126.03	85.89	58.45
RKo6s–SD3	53.39	39.68	29.61
RKo6s–SD4	32.22	25.10	19.73
RKo6s–SD5	25.46	19.11	15.18

Table 7
PPW for dissipation criterion $n = 10^6$.

	$\rho_{10^6} = 99.99\%$	$\rho_{10^6} = 99.9\%$	$\rho_{10^6} = 99\%$
RKo6s–SFo11p–FDo11p	87.70	59.55	40.26
RKo6s–CF8–CS6	40.26	28.89	21.06
RKo6s–SD2	185.17	126.14	85.86
RKo6s–SD3	70.83	52.88	39.54
RKo6s–SD4	41.97	32.08	25.04
RKo6s–SD5	36.73	25.52	19.11

Table 8
PPW for dissipation criterion $n = 10^7$.

	$\rho_{10^7} = 99.99\%$	$\rho_{10^7} = 99.9\%$	$\rho_{10^7} = 99\%$
RKo6s–SFo11p–FDo11p	128.96	87.69	59.50
RKo6s–CF8–CS6	57.46	40.25	28.87
RKo6s–SD2	271.85	185.19	126.06
RKo6s–SD3	94.57	70.61	52.80
RKo6s–SD4	57.36	41.92	32.05
RKo6s–SD5	54.66	36.74	25.51

Finally, the PPW criterion is now written as a function of the number of iterations and as a function of the accepted loss of accuracy in Table 5–8.

As expected, when the dissipation criterion is less restrictive, the number of PPW needed to discretise the signal decreases. For Spectral Difference schemes, when the polynomial order p increases, the number of PPW needed to discretise the signal decreases as well. The RKo6s–SFo11p–FDo11p needs more PPW than the RKo6s–CF8–CS6 according to this dissipation criterion. This fact could be explained by the accuracy of the associated filters (sixth-order versus eighth-order). Finally, the RKo6s–SD5 is equivalent to the RKo6s–CF8–CS6 in terms of dissipation.

5.5. Points per wavelength (PPW) – dispersion-based criterion

A cut-off wavenumber $k_c^\phi \Delta x$ associated with the phase shift error ϕ after n iterations can be defined in a similar way as for the dissipation-based criterion:

For a given set $(n, \nu, p) \in \left(\mathbb{N}^* \times \mathbb{R}^{+*} \times \mathbb{N}^* \right)$, look for

$$k\Delta x \in \left[0, k_c^\phi \Delta x \right] \text{ such that } \delta\varphi_n / 2\pi \, (k\Delta x, n, \nu, p) \leqslant \phi$$

This cut-off wavenumber can be obviously interpreted as a number of points per wavelength (PPW). The phase-based criterion is finally shown in Fig. 14 for both Finite Difference schemes, and for the Spectral Difference approach with p ranging from 2 to 5 and n from 10^4 to 10^7 at CFL number $\nu = 0.7$.

As before, the PPW criterion is now written as a function of the number of iterations and as a function of the accepted phase shift in Table 9–12.
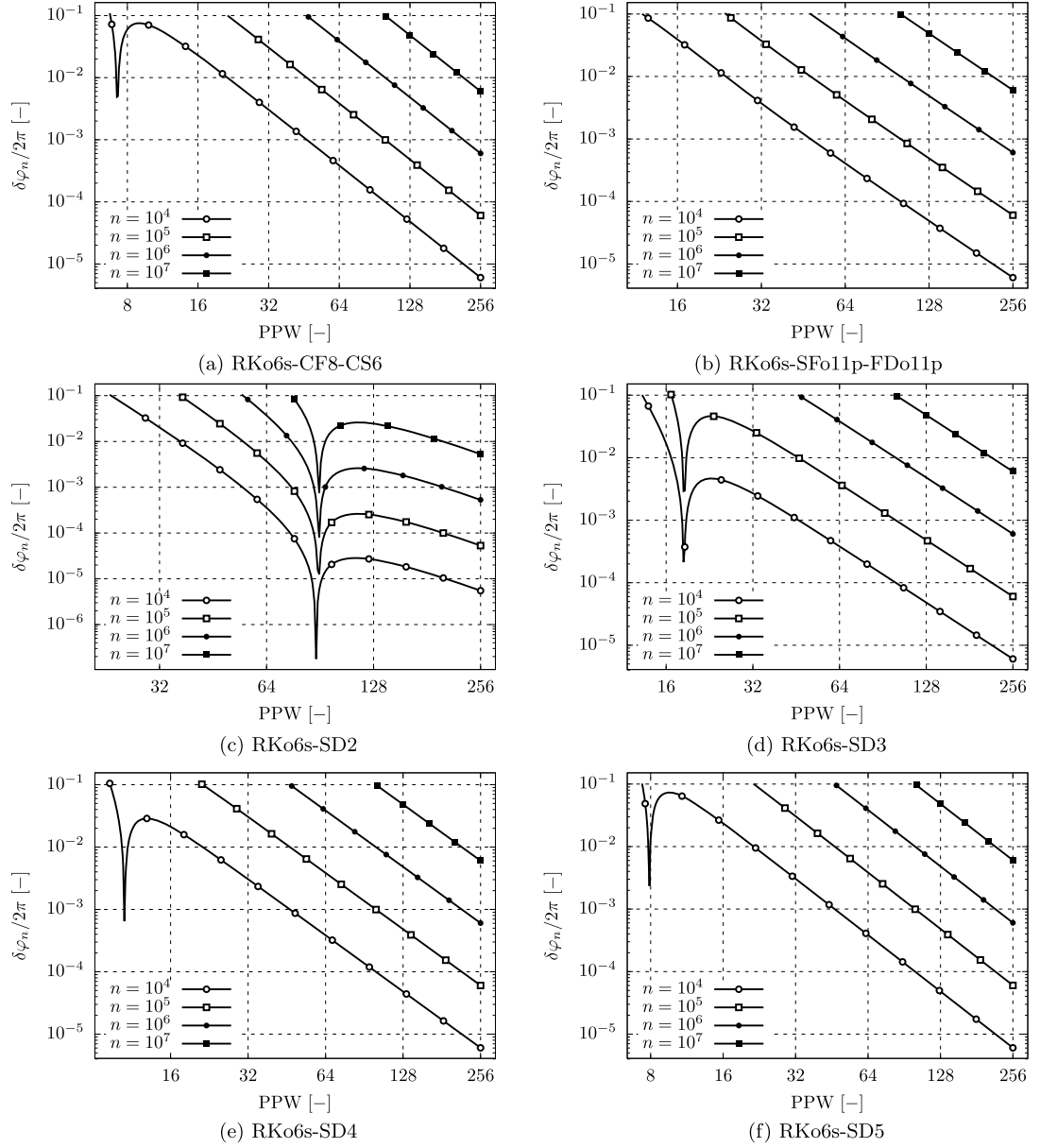
(a) RKo6s-CF8-CS6

(b) RKo6s-SFo11p-FDo11p

(c) RKo6s-SD2

(d) RKo6s-SD3

(e) RKo6s-SD4

(f) RKo6s-SD5

Fig. 14. Spectral analysis for $\nu = 0.7$: analysis of the phase-based criterion.

Table 9
PPW for dispersion criterion $n = 10^4$.

	$\delta\varphi_{10^4}/2\pi = 0.001$	$\delta\varphi_{10^4}/2\pi = 0.01$	$\delta\varphi_{10^4}/2\pi = 0.1$
RKo6s–SFo11p–FDo11p	48.07	23.86	11.95
RKo6s–CF8–CS6	46.51	21.39	6.76
RKo6s–SD2	54.78	36.56	23.38
RKo6s–SD3	46.09	16.65	13.21
RKo6s–SD4	46.51	21.31	9.32
RKo6s–SD5	46.52	21.45	7.38

As expected, when the dispersion criterion is less restrictive, the number of PPW needed to discretise the signal decreases. For Spectral Difference schemes, when the polynomial order p increases, the PPW needed to discretise the signal decreases as well except for pathological cases. This is due to the non-monotonic behaviour of dispersion curves, for example, for the RKo6s–SD2 with $n = 10^6$. The RKo6s–SFo11p–FDo11p approximatively needs the same number of PPW as

Table 10
PPW for dispersion criterion $n = 10^5$.

	$\delta\varphi_{10^5}/2\pi = 0.001$	$\delta\varphi_{10^5}/2\pi = 0.01$	$\delta\varphi_{10^5}/2\pi = 0.1$
RKo6s–SFo11p–FDo11p	101.14	48.07	23.86
RKo6s–CF8–CS6	100.34	46.51	21.39
RKo6s–SD2	75.16	54.96	36.61
RKo6s–SD3	100.30	46.07	16.66
RKo6s–SD4	100.34	46.51	21.31
RKo6s–SD5	100.34	46.52	21.46

Table 11
PPW for dispersion criterion $n = 10^6$.

	$\delta\varphi_{10^6}/2\pi = 0.001$	$\delta\varphi_{10^6}/2\pi = 0.01$	$\delta\varphi_{10^6}/2\pi = 0.1$
RKo6s–SFo11p–FDo11p	216.62	101.14	48.07
RKo6s–CF8–CS6	216.24	100.34	46.51
RKo6s–SD2	200.71	75.22	54.97
RKo6s–SD3	216.24	100.30	46.07
RKo6s–SD4	216.24	100.34	46.51
RKo6s–SD5	216.24	100.34	46.52

Table 12
PPW for dispersion criterion $n = 10^7$.

	$\delta\varphi_{10^7}/2\pi = 0.001$	$\delta\varphi_{10^7}/2\pi = 0.01$	$\delta\varphi_{10^7}/2\pi = 0.1$
RKo6s–SFo11p–FDo11p	466.08	216.62	101.14
RKo6s–CF8–CS6	465.91	216.24	100.34
RKo6s–SD2	459.89	200.68	75.22
RKo6s–SD3	465.90	216.24	100.30
RKo6s–SD4	465.91	216.24	100.34
RKo6s–SD5	465.91	216.24	100.34

Table 13
Computational cost τ in µs per iteration n and per Degree Of Freedom (DOF) for the three considered solvers. The computational cost τ (measured on a Intel Bi-Xeon E5-2660v3) is related to the simulation of an academic jet noise configuration when solving the complete Navier–Stokes equations.

CFD code	**JAGUAR**	**elsA**	**ALESIA**
Schemes	RKo6s-SD	RKo6s–CF8–CS6	RKo6s–SFo11p–FDo11p
Mesh	Unstructured	Structured	Structured
Approach	SD	FV	FD
τ [µs/n/DOF]	8	10	3

for the RKo6s–CF8–CS6 according to this dispersion criterion. Finally, the RKo6s–SD4 is equivalent to the RKo6s–CF8–CS6 in terms of dispersion.

5.6. Computational cost

The spectral analysis shows that the Spectral Difference method is a viable alternative to the standard aeroacoustic schemes for its accuracy. However, the interest is also motivated by the CPU cost associated with the method when solving the Navier–Stokes equations, since providing accurate results in a low restitution time is of utmost importance in an industrial setting.

The numerical methods of this paper are implemented in three different codes. The RKo6s–CF8–CS6 is implemented in the industrial **elsA** (standing for **e**nsemble **l**ogiciel de **s**imulation en **A**érodynamique) software of ONERA [41,42]. Even if the implementation is optimised, the performance attained is not the best one could obtain with a dedicated solver. In fact, **elsA** is a generic solver able to compute external aerodynamics and turbomachinery flows with RANS, URANS, LES and DES modelling. Such flexibility is associated with a CPU overhead per degree of freedom. The RKo6s–SFo11p–FDo11p is implemented in the **ALESIA** (standing for **A**ppropriate **L**arge **E**ddy **SI**mulation for **A**eroacoustics) in-house CFD code developed by Dr. Christophe Bogey [43] for research purpose. The code is optimised to run computations on massively parallel platforms. Such an optimised solver is likely to be providing the best performance. Finally, the Spectral Difference method is implemented in the **JAGUAR** (standing for pro**J**ect of an **A**erodynamic solver using **G**eneral **U**nstructured grids **A**nd high orde**R** schemes) code of CERFACS [44]. The structure of **JAGUAR** has been optimised in order to tackle the best CPU performance in serial and parallel computations, including OpenMP and MPI paradigms [45]. In particular, the restitution time [44] is shown to be only weakly sensitive to the polynomial degree p.

Table 13 demonstrates that the Spectral Difference method on unstructured grids is a viable alternative to the standard high-order schemes for aeroacoustics applied to structured grids. It opens a new research area for the application of this unstructured paradigm to problems of industrial relevance, including geometrical complexity.

6. Conclusions

The spectral analysis based on Fourier modes is one of the standard tools for defining the behaviour of a convection scheme. Injecting a solution projected onto the Fourier basis in the derivative, the exact and numerical approximation of the derivative can be compared, leading to a loss in amplitude (dissipation) and a phase-shift (dispersion). In this paper, we have revisited the spectral analysis focusing our attention on four aspects.

First, we account for the time discretisation in the analysis. Such an approach is applied to two sets of standard schemes for aeroacoustics simulations, the compact scheme of Lele and the DRP scheme of Bogey and Bailly (both with filters), while the time integration is performed with the second-order DRP scheme of Bogey and Bailly. The introduction of the time integration is shown to be able to have strong effects on the overall scheme capability, which results in changes in the standard Point-Per-Wavelength criterion. To the authors' knowledge, this first kind of result had never been highlighted before for the two proposed schemes.

Secondly, the space–time spectral analysis is applied to one of the spectral discontinuous schemes, namely the Spectral Difference scheme. The analysis shows that any solution is a combination of projected components on the set of eigenvectors. In the previous studies, one mode was referred to as a main mode and the others were called spurious. We think that this naming is prone to possible misunderstandings since the solution is always projected onto the whole set of eigenvalues / eigenvectors. Moreover, after simple algebraic simplifications, it is shown that the spectral behaviour is well-defined for wavenumbers in $[0, \pi]$ and aliasing always occurs for wavenumbers larger than π. Such a behaviour is general and valid for any high-order spectral discontinuous method. However, aliasing was not found in dissipation and dispersion figures published in the literature. Focusing on wavenumbers in $[0, \pi]$, since the Spectral Difference approach behaves as a solution projected onto a set of eigenvalues and eigenvectors, only the component associated with the eigenvector with the largest eigenvalue modulus is kept when the number of iterations to perform is large. For wavenumbers larger than π, aliasing always occurs. A naive conclusion would be to assume that spectral discontinuous methods are not competitive with respect to standard Finite Difference schemes applied in aeroacoustics: the cell size would be the same, but the number of degrees of freedom increases with the polynomial order p.

Thirdly, we were able to extend the space–time analysis for wavenumbers larger than π and we introduced two new criteria to define dissipation and dispersion. Dissipation is measured by an energy loss while dispersion is measured by a phase-shift. These new criteria are general enough to be applied to any kind of scheme, including (of course) Spectral Difference, Spectral Volume, Discontinuous Galerkin or Flux Reconstruction schemes. The criteria recover the standard criteria for any scheme with one degree of freedom per cell/mesh node. Figures related to both dissipation and dispersion were introduced for a range of polynomial order p and number of iterations, for a given CFL number and for a given input wavenumber.

Finally, the accuracy of standard Finite Difference and Spectral Difference schemes is compared. It is shown that the number of Points-Per-Wavelength of the compact scheme of Lele coupled with the time integration procedure and the associated filter is also obtained with the Spectral Difference scheme with $p = 5$ (sixth order of accuracy) in terms of dissipation and $p = 4$ (fifth order of accuracy) in terms of dispersion and the same time integration procedure. In fact, the spectral accuracy of the Lele's scheme coupled with the time integration and the filter is recovered by the Spectral Difference approach coupled with the same time integration procedure. To the best of our knowledge, it is the first time that a method for unstructured grids presents the same spectral accuracy as the compact scheme. As a consequence, it offers the numerical capability required in aeroacoustics computations. It is also shown using dedicated solvers that the CPU times per degree of freedom for the three considered approaches are of the same order of magnitude. Therefore, the SD method presents the same numerical efficiency as the standard Finite Difference schemes and the Spectral Difference method can be considered as an alternative to the Finite Difference schemes. Moreover the Spectral Difference method provides the additional flexibility of unstructured grids necessary to perform computations with complex geometries of industrial interest. Hence we plan to use the Spectral Difference method to perform aeroacoustics simulations for both academic and industrial configurations in a near future.

Appendix A. Details on the finite difference schemes

For the sake of consistency, we provide the coefficients related to the definition of the finite difference schemes.

Table 14
CF8 compact filter coefficients.

b_0	b_1	b_2	b_3	b_4
$\dfrac{93 + 70\alpha_f}{128}$	$\dfrac{7 + 18\alpha_f}{16}$	$\dfrac{-7 + 14\alpha_f}{32}$	$\dfrac{1 - 2\alpha_f}{16}$	$\dfrac{-1 + 2\alpha_f}{128}$

Table 15
FDo11p scheme and SFo11p filter coefficients.

(a) Coefficients of the fourth-order scheme FDo11p using 11 points with $a_{-j} = -a_j$ and $a_0 = 0$.		(b) Coefficients of the sixth-order filter SFo11p using 11 points with $d_{-j} = d_j$.	
a_1	0.872756993962	d_0	0.234810479761700
a_2	−0.286511173973	d_1	−0.199250131285813
a_3	0.090320001280	d_2	0.120198310245186
a_4	−0.020779405824	d_3	−0.049303775636020
a_5	0.002484594688	d_4	0.012396449873964
		d_5	−0.001446093078167

Table 16
Coefficients of the low-storage second-order six-stage Runge–Kutta (RKo6s) (see Eq. (6)).

γ_1	1.000000000000
γ_2	0.500000000000
γ_3	0.165919771368
γ_4	0.040919732041
γ_5	0.007555704391
γ_6	0.000891421261

Both CS6 and FDo11p schemes are centred and thus not dissipative. By applying a spatial Fourier transform to Eq. (2) and Eq. (4), the modified wavenumber k_m is obtained for the Lele's sixth-order compact schemes CS6 in Eq. (49) and for the fourth-order explicit scheme FDo11p in Eq. (50), respectively:

$$[k_m \Delta x]_{\text{CS6}} = \frac{\dfrac{14}{9} \sin(k\Delta x) + \dfrac{1}{18} \sin(2k\Delta x)}{1 + \dfrac{2}{3} \cos(k\Delta x)}, \tag{49}$$

$$[k_m \Delta x]_{\text{FDo11p}} = 2 \sum_{l=1}^{5} a_j \sin(l k \Delta x). \tag{50}$$

On the contrary, the filters only introduce dissipation and do not create any dispersion. When a Fourier mode is considered as an initial solution, the dissipation rates $\mathcal{F} = u_i^f / u_i$ obtained for the eighth-order compact filter CF8 and for the sixth-order explicit filter SFo11p are defined respectively by:

$$[\mathcal{F}(k\Delta x)]_{\text{CF8}} = \frac{1}{1 + 2\alpha_f \cos(k\Delta x)} \sum_{l=0}^{4} b_l \cos(l k \Delta x), \tag{51}$$

$$[\mathcal{F}(k\Delta x)]_{\text{SFo11p}} = 1 - \sigma_d d_0 - 2\sigma_d \sum_{l=1}^{5} d_l \cos(l k \Delta x). \tag{52}$$

Appendix B. Details on the spectral difference method

The spectral difference method solves the strong form of the equations using the sets of solution and flux points. Here, the explanation related to the position of the degrees of freedom is performed in $[-1, 1]$, since any 1D cell can be cast into $[-1, 1]$ by an isoparametric transformation.

The unknown polynomial for u is totally defined by its values at the *solution points* and here, the solution points are selected as the roots of the Chebyshev polynomial (of the first kind) of degree p defined by:

$$SP_l = -\cos\left(\frac{2l-1}{2p+2}\pi\right) \text{ for } 1 \leqslant l \leqslant p+1. \tag{53}$$

It is shown in [28] that the SD approach is independent of the solution point location and our choice is given for completeness.

The flux polynomial is defined by $p+2$ *flux points* (1 point more than the solution). Following Kopriva and Kolias [9], two flux points are located at the segment boundaries and any other p flux point is located between two solution points. The approach is staggered. In this paper, we choose the p flux points as the roots of the Legendre polynomials of degree p and the two segment end points, as Huynh [18]. We found that this choice is the best one for stability and in particular, the other standard choice (Chebyshev–Gauss–Lobatto) is proved to be weakly unstable for $p > 2$ [28,46].

Both solution and flux polynomials are based on the Lagrange polynomials using the solution points SP_l and the flux points FP_l respectively. The Lagrange polynomials $\mathcal{L}_l$ of degree p based on the solution point index l is:

$$\mathcal{L}_l(x) = \prod_{\substack{r=1 \\ r \neq l}}^{p+1} \frac{x - SP_r}{SP_l - SP_r} \tag{54}$$

and the solution in cell i $u_i(x,t)$ can be expanded over this basis as:

$$u_i(x,t) = \sum_{l=1}^{p+1} u_i(SP_l, t)\,\mathcal{L}_l(x). \tag{55}$$

In the same way, the Lagrange polynomials $\mathcal{T}_l$ of order $p+1$ based on the flux point index l is:

$$\mathcal{T}_l(x) = \prod_{\substack{r=1 \\ r \neq l}}^{p+2} \frac{x - FP_r}{FP_l - FP_r} \tag{56}$$

and the flux function polynomial $f_i(x,t)$ in cell i ($f_i(x,t) = cu_i(x,t)$ for the advection equation) can be expanded over the basis as:

$$f_i(x,t) = \sum_{l=1}^{p+2} f_i(FP_l, t)\,\mathcal{T}_l(x). \tag{57}$$

The SD procedure is now as follows. First, the solution is extrapolated at the flux point locations using Eq. (55). At the interior flux points, the flux is computed immediately from the solution. The flux on border flux points is the solution of a Riemann problem since the two extrapolated quantities (one at each side) can differ. Finally, the divergence of the flux polynomial is evaluated at the solution point locations by differentiation of Eq. (57) as:

$$\frac{\partial f_i}{\partial x}(x,t) = \sum_{l=1}^{p+2} f_i(FP_l, t)\,\mathcal{T}_l'(x), \text{ where } \mathcal{T}_l'(x) = \frac{d\mathcal{T}_l}{dx}(x). \tag{58}$$

References

[1] M.M. Rai, P. Moin, Direct simulations of turbulent flow using finite-difference schemes, J. Comput. Phys. 96 (1) (1991) 15–53.
[2] S.K. Lele, Compact finite difference schemes with spectral-like resolution, J. Comput. Phys. 103 (1992) 16–42, http://dx.doi.org/10.1016/0021-9991(92)90324-R.
[3] C.K. Tam, J.C. Webb, Dispersion–relation–preserving finite difference schemes for computational acoustics, J. Comput. Phys. 107 (2) (1993) 262–281, http://dx.doi.org/10.1006/jcph.1993.1142.
[4] W. Reed, T. Hill, Triangular Mesh Methods for the Neutron Transport Equation, Tech. Report LU-UR-73-279, Los Alamos National Laboratory, New Mexico, USA, 1973.
[5] B. Cockburn, C. Shu, TVB Runge–Kutta local projection discontinuous Galerkin finite method for conservation laws II: general framework, Math. Comput. 52 (186) (1989) 411–435.
[6] B. Cockburn, S. Lin, C. Shu, TVB Runge–Kutta local projection discontinuous Galerkin finite element method for conservation laws III: one-dimensional systems, J. Comput. Phys. 84 (1989) 90–113.
[7] B. Cockburn, S. Hou, C. Shu, The Runge–Kutta local projection discontinuous Galerkin finite element method for conservation laws IV: the multidimensional case, Math. Comput. 54 (1990) 545–581.
[8] J. Hesthaven, T. Warburton, Nodal Discontinuous Galerkin Methods – Algorithms, Analysis and Applications, Springer, 2008.
[9] D. Kopriva, J. Kolias, A conservative staggered-grid Chebyshev multidomain method for compressible flows, J. Comput. Phys. 125 (1) (1996) 244–261.
[10] Y. Liu, M. Vinokur, Z. Wang, Spectral difference method for unstructured grids I: basic formulation, J. Comput. Phys. 216 (2) (2006) 780–801.
[11] Z. Wang, Y. Liu, G. May, A. Jameson, Spectral difference method for unstructured grids II: extension to the Euler equations, J. Sci. Comput. 32 (2007) 45–71.

[12] C. Liang, A. Jameson, Z. Wang, Spectral difference method for compressible flow on unstructured grids with mixed elements, J. Comput. Phys. 228 (8) (2009) 2847–2858.
[13] Z. Wang, Spectral (finite) volume method for conservation laws on unstructured grids: basic formulation, J. Comput. Phys. 178 (1) (2002) 210–251.
[14] Z. Wang, Y. Liu, Spectral (finite) volume method for conservation laws on unstructured grids II: extension to two-dimensional scalar equation, J. Comput. Phys. 179 (2) (2002) 665–697.
[15] Z. Wang, Y. Liu, Spectral (finite) volume method for conservation laws on unstructured grids III: one dimensional system and partition optimization, J. Sci. Comput. 20 (2004) 137–157.
[16] Z. Wang, L. Zang, Y. Liu, Spectral (finite) volume method for conservation laws on unstructured grids IV: extension to two-dimensional systems, J. Comput. Phys. 194 (2) (2004) 716–741.
[17] Y. Liu, M. Vinokur, Z. Wang, Spectral (finite) volume method for conservation laws on unstructured grids V: extension to three-dimensional systems, J. Comput. Phys. 212 (2) (2006) 454–472.
[18] H. Huynh, A flux reconstruction approach to high-order schemes including discontinuous Galerkin methods, in: 18th AIAA Computational Fluid Dynamics Conference, 25–28 June, Miami, FL, 2007, AIAA Paper 2007-4079.
[19] Z. Wang, H. Gao, A unifying lifting collocation penalty formulation including the discontinuous Galerkin, spectral volume/difference methods for conservation laws on mixed grids, J. Comput. Phys. 228 (21) (2009) 8161–8186.
[20] P. Vincent, P. Castonguay, A. Jameson, A new class of high-order energy stable flux reconstruction schemes, J. Sci. Comput. 47 (1) (2011) 50–72.
[21] P. Castonguay, P. Vincent, A. Jameson, A new class of high-order energy stable flux reconstruction schemes for triangular elements, J. Sci. Comput. 51 (2012) 224–256.
[22] H. Huynh, Z. Wang, P. Vincent, High-order methods for computational fluid dynamics: a brief review of compact differential formulations on unstructured grids, Comput. Fluids 98 (2014) 209–220.
[23] Y. Allaneau, A. Jameson, Connections between the filtered discontinuous Galerkin method and the flux reconstruction approach to high order discretizations, Comput. Methods Appl. Mech. Eng. 200 (2011) 3626–3636.
[24] R. Vichnevetsky, J. Bowles, Fourier Analysis of Numerical Approximation of Hyperbolic Equations, SIAM Studies in Applied Mathematics, 1982.
[25] F. Hu, M. Hussaini, P. Rasetarinera, An analysis of the discontinuous Galerkin method for wave propagation problems, J. Comput. Phys. 151 (1999) 921–946.
[26] M. Zhang, C. Shu, An analysis of three different formulations of the discontinuous Galerkin method for diffusion equations, Math. Methods Appl. Sci. 13 (3) (2003) 395–414.
[27] R. Kannan, Z. Wang, LGD2: a variant of the LDG flux formulation for the spectral volume method, J. Sci. Comput. 46 (2011) 314–328.
[28] K. Van den Abeele, C. Lacor, Z. Wang, On the stability and accuracy of the spectral difference method, J. Sci. Comput. 37 (2008) 162–188.
[29] P. Vincent, P. Castonguay, A. Jameson, Insights from von Neumann analysis of high-order flux reconstruction schemes, J. Comput. Phys. 230 (22) (2011) 8134–8154.
[30] K. Asthana, A. Jameson, High-order flux reconstruction schemes with minimal dispersion and dissipation, J. Sci. Comput. 62 (3) (2015) 913–944, http://dx.doi.org/10.1007/s10915-014-9882-5.
[31] C. Bogey, C. Bailly, A family of low dispersive and low dissipative explicit schemes for flow and noise computations, J. Comput. Phys. 194 (1) (2004) 194–214, http://dx.doi.org/10.1016/j.jcp.2003.09.003.
[32] D. Gaitonde, M. Visbal, Further development of a Navier–Stokes solution procedure based on higher-order formulas, in: 37th AIAA Aerospace Sciences Meeting, January, Reno, Nevada, 1999, AIAA Paper 1999-557.
[33] K.M. Aikens, N.S. Dhamankar, C.S. Martha, Y. Situ, G.A. Blaisdell, Equilibrium wall model for large eddy simulations of jets for aeroacoustics, in: AIAA SciTech, 52nd Aerospace Sciences Meeting, 13–17 January, National Harbor, Maryland, 2014, AIAA Paper 2014-0180.
[34] S. Le Bras, H. Deniau, C. Bogey, G. Daviller, Development of compressible large-eddy simulations combining high-order schemes and wall modeling, in: AIAA Aviation 21st AIAA/CEAS Aeroacoustics Conference, 22–26 June, Dallas, TX, 2015, AIAA Paper 2015-3135.
[35] C. Bogey, N. de Cacqueray, C. Bailly, A shock-capturing methodology based on adaptative spatial filtering for high-order non-linear computations, J. Comput. Phys. 228 (5) (2009) 1447–1465, http://dx.doi.org/10.1016/j.jcp.2008.10.042.
[36] J. Ramboer, T. Broeckhoven, S. Smirnov, C. Lacor, Optimization of time integration schemes coupled to spatial discretization for use in CAA applications, J. Comput. Phys. 213 (2) (2006) 777–802.
[37] T. Sengupta, A. Dipankar, P. Sagaut, Error dynamics: beyond von Neumann analysis, J. Comput. Phys. 226 (2007) 1211–1218.
[38] T. Sengupta, High Accuracy Computing Methods: Fluid Flows and Wave Phenomena, Cambridge University Press, 2013.
[39] O. Axelsson, Iterative Solution Methods, Cambridge University Press, 1996.
[40] G. Golub, C. Van Loan, Matrix Computations, 3rd ed., Johns Hopkins University Press, Baltimore, MD, USA, 1996.
[41] L. Cambier, S. Heib, S. Plot, The Onera elsA CFD software: input from research and feedback from industry, Mech. Ind. 14 (3) (2013) 159–174, http://dx.doi.org/10.1051/meca/2013056.
[42] A. Fosso Pouangué, H. Deniau, F. Sicot, P. Sagaut, Curvilinear finite-volume schemes using high-order compact interpolation, J. Comput. Phys. 229 (13) (2010) 5090–5122, http://dx.doi.org/10.1016/j.jcp.2010.03.027.
[43] C. Bogey, C. Bailly, D. Juvé, Computation of flow noise using source terms in linearized Euler's equations, AIAA J. 40 (2) (2002) 235–243.
[44] A. Cassagne, J.-F. Boussuge, N. Villedieu, G. Puigt, I. D'Ast, A. Genot, JAGUAR: a new CFD code dedicated to massively parallel high-order LES computations on complex geometry, in: 50th 3AF International Conference on Applied Aerodynamics, Toulouse, France, 2015.
[45] A. Cassagne, G. Puigt, J. Boussuge, High-Order Method for a New Generation of Large Eddy Simulation Solver, Tech. Rep., Partnership for Advanced Computing in Europe (PRACE), available online at www.prace-ri.eu, 2015.
[46] A. Jameson, A proof of the stability of the spectral difference method for all orders of accuracy, J. Sci. Comput. 45 (2010) 348–358.